DIRECT GENOME EDITING OF PATIENT-DERIVED XENOGRAFTS USING CRISPR-CAS9 ENABLES RAPID *IN VIVO* FUNCTIONAL GENOMICS

by

Christopher Hron Hulton

A Dissertation

Presented to the Faculty of the Louis V. Gerstner Jr.

Graduate School of Biomedical Sciences,

Memorial Sloan Kettering Cancer Center

in Partial Fulfillment of the Requirements for the Degree of

Doctor of Philosophy

New York, NY

September, 2019

_____ _____

Charles M. Rudin, MD, PhD
Dissertation Mentor

Date

To Kendra, for all her love and support

ABSTRACT

Patient-derived xenografts are clinically relevant *in vivo* cancer models that maintain the molecular characteristics of their tumors of origin. In contrast to either cancer cell lines or genetically engineered mouse models, the utility of PDXs has been limited by the inability to perform targeted genome editing of these tumors. Here, we developed a series of vectors enabling CRISPR-Cas9 editing of PDXs. The main focus of this platform is pSpCTRE, a tightly regulated, doxycycline-inducible Cas9 lentiviral vector that does not require *in vitro* culture for selection of transduced cells. Additionally, pSpCTRE includes a novel cell surface reporter of dox-induced Cas9 expression to robustly identify cells that undergo Cas9-mediated genome editing. We next developed sgTrack, an sgRNA expression vector with a flexible reporter system for tracking clonal dynamics of sgRNA populations and a recombinant AAV vector to simultaneously deliver and sgRNA and DNA repair template to precisely edit cells by homology-directed repair. We verified through *in vitro* experimentation that these vectors display the properties necessary to perform *in vivo* genome editing experiments.

Using this platform, we generated a library of SpCTRE PDXs representing multiple lung cancer subtypes that inducibly express Cas9. Through disruption of the essential gene *RPA1* or the *KRAS* proto-oncogene, we found that SpCTRE PDXs are well suited to identify *in vivo* genetic dependencies. We also demonstrated the ability of this platform to analyze mechanisms of acquired drug

resistance by introducing the osimertinib resistance mutation $EGFR^{C797S}$ into an EGFR-mutant adenocarcinoma PDX using templated homology-directed repair. This flexible system has broad application to other explant models and substantially augments the utility of PDXs as genetically programmable models of human cancer.

ACKNOWLEDGEMENTS

First, I would like to thank Dr. Charles Rudin and Dr. JT Poirier for their mentorship through my PhD. I am very grateful for your trust in me and for continuing to challenge me to grow as a scientist over the last 5 years.

Thank you to all past and present members of the Rudin lab for all of their help and guidance over the past 5 years. I would especially like to thank Eric Gardner and Linde Miles for welcoming me into the lab during my rotation and making it impossible for me to consider joining any other lab. To the countless other people I've cross paths with in the lab, whether for 5 years or 5 minutes, it was truly an enjoyable experience working with all of you.

I would like to thank the members of my thesis committee, Dr. Neal Rosen and Dr. Andrea Ventura, for their advice and accessibility throughout my PhD.

Thank you to my classmates Steve Albanese, Jake Boyer, Nayan Jain, Nick Kuhn, Xiaoyi Li, Michelle Riegman, Ben Tischler, and Yuchen Xie for making our time together at GSK as entertaining and fun as it could be. It was an unbelievable experience that I will not soon forget.

I am thankful for the incredible environment that exists at GSK, which has been cultivated by so many people over the years. Thank you to Ken Marians,

Michael Overholtzer, Linda Burnley, Iwona Abramek, Maria Torres, Ivan Gerena, and David McDonagh for everything you've done to make GSK an amazing graduate program.

Lastly, I would like to thank my parents, Peter and Carol, as well as my girlfriend, Kendra Bissonnette, and her parents, Mike and Jeanne. This truly would not have been possible if not for their unwavering support and encouragement in so many different ways. Thank you all so much.

LIST OF TABLES

LIST OF FIGURES

LIST OF ABBREVIATIONS

4-HT: 4-hydroxytamoxifen

C/O: crizotinib-osimertinib

Cas9: CRISPR associated 9

$CD4^T$: truncated CD4

CDX: CTC-derived xenograft

cPPT: central polypurine tract

CRISPR: clustered regularly interspaced short palindromic repeats

crRNA: CRISPR RNA

CTC: circulating tumor cell

dCas9: catalytically dead Cas9

dgRNA: dead sgRNA

Dox: doxycycline

DSB: double strand break

EFS: EF-1α short

FACS: fluorescence-activated cell sorting

GEMM: genetically engineered mouse model

HDR: homology-directed repair

LTR: long terminal repeat

MACS: magnetic-activated cell sorting

NHEJ: non-homologous end joining

NIBR PDXE: Novartis Institute for BioMedical Research PDX encyclopedia

NK: natural killer

NSG: non-obese diabetic-severe combined immunodeficiency-gamma

PAM: proto-spacer adjacent motif

PDO: patient-derived organoid

PDX: patient-derived xenograft

pSpCTRE: *Streptococcus pyogenes* Cas9-Tet Response Element

rAAV: recombinant adeno-associated virus

RCT: randomized clinical trial

RNP: ribonucleoprotein

rtTA: reverse tetracycline transcriptional activator

SCLC: small cell lung cancer

sgRNA: single guide RNA

Tet: tetracycline

TetR: tetracycline-responsive repressor

TIDE: tracking of indels by decomposition

TKI: tyrosine kinase inhibitor

TRE: tetracycline response element

tracrRNA: trans-activating CRISPR RNA

UMI: unique molecular identifier

WPRE: woodchuck hepatitis virus post-transcriptional regulatory element

CHAPTER 1

INTRODUCTION

Cancer is a worldwide public health problem and a leading cause of death in the United States with an estimated 600,000 deaths expected to occur in 2019 alone (Siegel et al., 2019). While overall mortality rates are decreasing, a greater understanding of these diseases is necessary to enhance patient outcomes and accelerate this decline. Cancer is fundamentally caused by genetic alterations that cause normal cells to transform into cancerous cells with sustained proliferation, immune evasion, and altered metabolism, along with other hallmark features of malignancy (Hanahan et al., 2011). Cancer models allow researchers to study these hallmark features in a laboratory setting to better understand the molecular origins of cancer and develop improved therapeutic strategies aimed at increasing tumor response rates and overcoming drug resistance. The utility of these models is solely defined by how well they replicate the biology of human tumors and, therefore, enable clinically relevant discoveries (Ben-David et al., 2017). Patient-derived xenografts (PDXs) are a clinically relevant model system that faithfully recapitulate several features of human tumors, yet technical barriers prevent their use in many research applications (Hidalgo et al., 2014; Siolas and Hannon, 2013). In my thesis, I sought to develop a genome editing platform for use in PDXs that would enhance their value in preclinical cancer research.

Patient-Derived Xenografts

PDXs are *in vivo* cancer models whereby human tumor cells are directly engrafted into immunodeficient mice in the hopes that the continued *in vivo* growth of the human tumor in a mouse will mimic tumor growth in the patient (Pillai and Uthamanthil, 2016). Remarkably, these models were first generated more than 50 years ago and it was appreciated then that PDX tumors resembled the primary tumor from which they were derived (Cobb, 1973; Rygaard and Povlsen, 1969). However, the contemporaneous development of *in vitro* cell line models prevented the widespread adoption of PDXs (Pillai and Uthamanthil, 2016). Cell lines are cheaper to maintain, offer more consistent growth characteristics and, in many cases, can also be grown as xenografts in immunodeficient mice (Fogh et al., 1977; Giovanella et al., 1972). Thus, cells lines were favored over PDXs as the predominant cancer model of the late 1900s (Pillai and Uthamanthil, 2016).

Nonetheless, PDXs have re-emerged over the last 20 years as important cancer models, owing largely to the inadequacies of cell line models identified over that time. Beginning with an analysis by Johnson and colleagues, it has become clear that cell lines and cell line xenografts have a limited ability to predict therapeutic efficacy in the clinic (Johnson et al., 2001; Kung, 2007). Potentially underlying this is the permanent alteration of cell lines that occurs as they adapt to the selective pressure of *in vitro* growth, which causes them to no longer share important characteristics with their tumor of origin (Daniel et al., 2009). By circumventing the problem of *in vitro* selection, PDXs may better

recapitulate many key aspects of human tumors, supporting their particular value as models for numerous preclinical research applications (Hidalgo et al., 2014).

Generation of PDXs

Creating PDX models begins with the collection of human tumor specimens, which can be achieved through surgical resection, biopsy, or collection of tumor cell-containing fluids such as pericardial, pleural, or peritoneal effusions (Mattar et al., 2016). Recently, circulating tumor cells (CTCs) collected from blood samples have been used to successfully generate PDXs (sometimes referred to as CTC-derived xenografts or CDXs) (Hodgkinson et al., 2014; Lallo et al., 2017; Morrow et al., 2016). Cells are most commonly engrafted subcutaneously as either a tumor fragment or single-cell suspension, depending on the source and amount of material obtained (Williams et al., 2013). The likelihood that a tumor will grow from the engrafted cells is highly variable and depends the sample quality as well as the time between specimen collection and subsequent implantation (Guerrera et al., 2016). It has been observed that successful PDX engraftment predicts a poorer clinical outcome, which perhaps indicates that aggressive tumors can more readily adapt to subcutaneous growth (John et al., 2011; Oh et al., 2015). Importantly, once a PDX is established from the primary tumor specimen, it can usually be serially transplanted into additional mice for expansion, cryo-preservation, and experimentation (Mattar et al., 2016).

PDXs necessitate the use of immunodeficient mice as endogenous murine immune cells would otherwise recognize human tumor cells as foreign and

prevent tumor outgrowth (Hirenallur-Shanthappa et al., 2016). Several strains of mice have been developed that can support xenograft tumor growth, beginning with the fortuitous discovery of the Nude mouse (Flanagan, 1966). These mice were determined to be athymic and T cell deficient (Pantelouris, 1968), which was later traced to a mutation in the *Foxn1* gene. However, nude mice still retain B cells and innate immune cells, thus they are only partially immunodeficient (Hirenallur-Shanthappa et al., 2016). Many subsequent mutations have been identified that affect development of the murine immune system and these have been leveraged to create additional strains of immunodeficient mice. Of note, the *Prkdc*^{scid} mutation prevents V(D)J recombination necessary for T- and B- cell development and *IL2rγ*^{null} mutations block signaling from IL-2 and other cytokines important for both adaptive and innate immune responses (Hirenallur-Shanthappa et al., 2016). These two mutations in the nonobese diabetic (NOD) background create the NSG (NOD-SCID-gamma) mouse strain. NSG mice are strongly immunodeficient as they lack T cells, B cells, and natural killer (NK) cells in addition to impaired macrophage and dendritic cell function (Agliano et al., 2008; Ishikawa et al., 2005).

The choice of mouse strain is an important consideration for PDXs as it has been shown that the engraftment rate is higher in more strongly immunodeficient mice (McDermott et al., 2010; Quintana et al., 2008). For this reason, NSGs are most commonly used mouse strain for PDXs, however, immunodeficient mice with further decreased antitumor immunity are under active development (Hirenallur-Shanthappa et al., 2016). Once established in

NSG mice, many PDX models can be successfully transplanted into Nude mice to allow at least partial analysis of tumor cell interaction with innate immune effectors.

Molecular features and utility of PDXs

A fundamental question concerning the use of PDXs is to what extent do these models recapitulate the biology of human tumors (Aparicio et al., 2015)? While this is a difficult question to answer directly, several studies have reported close preservation of histopathology characteristics and IHC expression patterns in PDXs across several tumor types reflective of their donor tumors (Hidalgo et al., 2014). More detailed analyses comparing the gene expression, epigenetic, and mutational profiles of PDXs to both primary tumors and cell lines have highlighted that PDXs match the molecular profiles of their tumors of origin more closely than cell line models (Daniel et al., 2009; DeRose et al., 2011; Drapkin et al., 2018; Fichtner et al., 2008; Poirier et al., 2015; Sivanand et al., 2012). One study of more than 1000 PDXs in the Novartis Institute for BioMedical Research PDX encyclopedia (NIBR PDXE) found the mutational and copy-number landscape to be closely correlated between PDXs and clinical samples and greater than the correlation between cell lines and clinical samples (Gao et al., 2015). These findings emphasize that, while no perfect model of human tumors exists, PDXs resemble the molecular features and histopathology characteristics of primary tumors more accurately than cell line-based cancer models (Aparicio et al., 2015; Hidalgo et al., 2014).

PDXs have proven to be exceptional surrogates for evaluating the clinical efficacy of cancer therapeutics (Hidalgo et al., 2014; Rosfjord et al., 2014). A study of small cell lung cancer (SCLC) PDXs found a close correlation between patient treatment history and response to chemotherapy; PDXs from treatment naïve patients were highly chemosensitive and PDXs from pre-treated patients showed a range of responses and were generally chemoresistant (Drapkin et al., 2018). This mirrors the clinical response of SCLC patients to chemotherapy and, surprisingly, this relationship was not observed in a similar study of SCLC cell lines (Polley et al., 2016). Another study of solid tumor PDXs showed that both positive and negative patient responses to therapy were accurately replicated by the PDX models derived from these patients (Izumchenko et al., 2017). Large scale PDX collections employed in randomized clinical trial (RCT)-like experiments have further demonstrated the power of these models to predict therapeutic success (or failure) in patients (Bruna et al., 2016; Gao et al., 2015; Krepler et al., 2017; Townsend et al., 2016).

The clinical relevance of PDXs provides numerous opportunities for additional translation research applications. Therapeutic studies in PDXs are strengthened by accompanying genomic analyses directed at identifying biomarkers of therapeutic response or resistance (Bertotti et al., 2011; Fichtner et al., 2008). It is also possible to generate multiple PDXs from the same patient to study their disease progression over time or to compare tumor characteristics and therapeutic response in PDXs derived from primary and metastatic sites (Gandara et al., 2015). This is especially true for CTC-derived PDXs, as blood

collection is a non-invasive method for accessing tumor cells that can be performed repeatedly (Lallo et al., 2017). Finally, PDXs are commonly used to model mechanisms of adaptive resistance and identify new therapeutic liabilities in resistant tumors (Cottu et al., 2014; Gardner et al., 2017; Monsma et al., 2015). These applications underscore the utility of PDXs in discovering clinically meaningful aspects of cancer biology.

Recently, patient-derived organoids (PDOs) have been reported to share many of the same characteristics as PDXs with respect to modeling human cancer (Tuveson and Clevers, 2019). These include mirroring the genetics of the tumor of origin (Weeber et al., 2015) and recapitulating patient drug responses (Lee et al., 2018; Vlachogiannis et al., 2018). As PDOs are grown in culture, they are easier to manipulate and expand than PDXs, however, this also represents a limitation for these models, as several aspects of the *in vivo* tumor environment are not recapitulated. Namely, PDOs are grown in an environment with excess nutrients, which does not reflect the competitive environment of human tumors, and drug studies in culture can be performed with non-physiological drug concentrations that are exempt from pharmacokinetic constraints. Yet, PDOs can be cocultured with human immune cells to evaluate and optimize immunotherapy response (Dijkstra et al., 2018; Neal et al., 2018). These features of PDOs highlight that they can serve as important models to complement PDXs in elucidating human tumor biology and in developing improved patient treatment strategies.

Limitations

While PDXs exhibit strong clinical relevance, several research applications remain out of reach due to inherent limitations of this model system. Most notably, PDXs display a vastly different tumor microenvironment than human tumors as 1) human stroma cells are replaced by murine stroma in the first few passages after PDX engraftment (Schneeberger et al., 2016) and 2) immune cells are generally absent due to the requirement for a highly immunosuppressed host. This largely prevents the use of PDXs for evaluating cancer immunotherapies since these studies generally must be performed in the context of an intact immune system (Choi et al., 2018). However, several strains of immunodeficient mice have been adapted to contain various components of the human immune system through genetic engineering or adoptive transfer of donor hematopoietic cells or tissue (Eswaraka and Giddabasappa, 2016). Although still an emerging technology, these humanized mice are increasingly being used with established PDXs to enable preclinical cancer immunotherapy studies (Wang et al., 2018; Zhao et al., 2018).

PDXs are not exempt from the selective pressures of clonal selection and genetic drift that drive cancer models away from faithfully representing their tumor of origin (Ben-David et al., 2019). Clonal heterogeneity is a defining feature of human cancer and capturing this intratumoral heterogeneity is important for modeling tumor evolution, metastasis, therapeutic efficacy, and resistance (McGranahan and Swanton, 2017). The extent of clonal selection during PDX engraftment varies widely, but this selection process can

substantially alter the clonal architecture of the resulting tumor and therefore affect functional studies (Ben-David et al., 2017; Eirew et al., 2015). However, aggressive tumors with low clonal diversity, such as SCLC, may not experience this selective pressure to the same extent (Drapkin et al., 2018; Poirier et al., 2015). Importantly, minimal genetic drift occurs across PDX passages suggesting that these models are genomically stable once they are established in the mouse (Ben-David et al., 2017; Bruna et al., 2016).

It has long been proposed that PDXs could serve as patient "avatars": laboratory models exactly replicating a patient's disease in which therapeutic combinations could be tested and refined to develop personalized treatment strategies (Malaney et al., 2014). Although an appealing premise, there are numerous hurdles that would need to be overcome to bring this idea to fruition. It was appreciated with early PDX models that the time required to establish PDXs often exceeded patient survival and thus, these models could not be used to inform clinical treatment strategies (Shorthouse et al., 1980). Additionally, limited engraftment rates for PDXs further decreases the number of patients who might benefit from this approach (Hidalgo et al., 2014). While these features of PDXs in theory could be improved, they represent significant technical barriers for the patient avatar approach.

PDXs are typically implanted heterotopically as subcutaneous flank tumors rather than orthotopically in their tissue of origin because tumors grown in the flank of a mouse are easier to monitor and do not require complex surgery to implant (Mattar et al., 2016). However, subcutaneous PDXs experience an

artificial environment, which does not resemble that of human tumors and can alter the tumor characteristics. A striking example of this is the impaired metastatic potential of subcutaneous tumors, which rarely metastasize and is contrasted by the high rate of metastasis observed for orthotopic PDXs (Hoffman, 2015). Additionally, the tumor microenvironment can affect therapeutic response and this may not be adequately modeled by subcutaneous PDXs (Calles et al., 2013). Despite the barriers to orthotopic implantation, these models may out perform traditional subcutaneous PDXs in recapitulating several aspects of human tumors.

Finally, a significant technical limitation for PDXs is the inability to genetically manipulate these models. The continuous *in vivo* growth of PDXs prevents their use with antibiotic selection methods developed specifically for *in vitro* models (Siolas and Hannon, 2013). Overcoming this limitation and performing genome editing experiments in PDXs is the focus for this thesis.

Rudin lung cancer PDX library

Lung cancer, while decreasing in incidence, remains the leading cause of cancer deaths in the United States (Siegel et al., 2019). Lung cancer is a molecularly heterogeneous disease that is broadly divided into non-small cell lung cancer (NSCLC) and small cell lung cancer (SCLC), with further subdivisions based on histology and genomic alterations that inform clinical treatment strategies (Gazdar et al., 2017; Herbst et al., 2018). Since 2004, the Rudin lab has engrafted more than 1400 lung cancer specimens and

successfully established over 300 lung cancer PDXs (Fig. 1.1a). Consistent with general incidence rates, the most commonly represented lung cancer subtypes in this collection are adenocarcinoma, SCLC, and squamous cell carcinoma, although rare subtypes such as mesothelioma and sarcomatoid carcinoma are also represented (Fig. 1.1b). Specimens for generating PDXs are collected from primary and metastatic sites using a variety of techniques (Fig. 1.1c, d). Some recent examples of the use of PDXs from this collection include modeling therapeutic resistance in SCLC (Gardner et al., 2017), evaluating a novel combination therapy for KRAS-mutant adenocarcinoma (Manchado et al., 2016), and assessing metabolic vulnerabilities in KEAP1-mutant lung cancer (Romero et al., 2017).

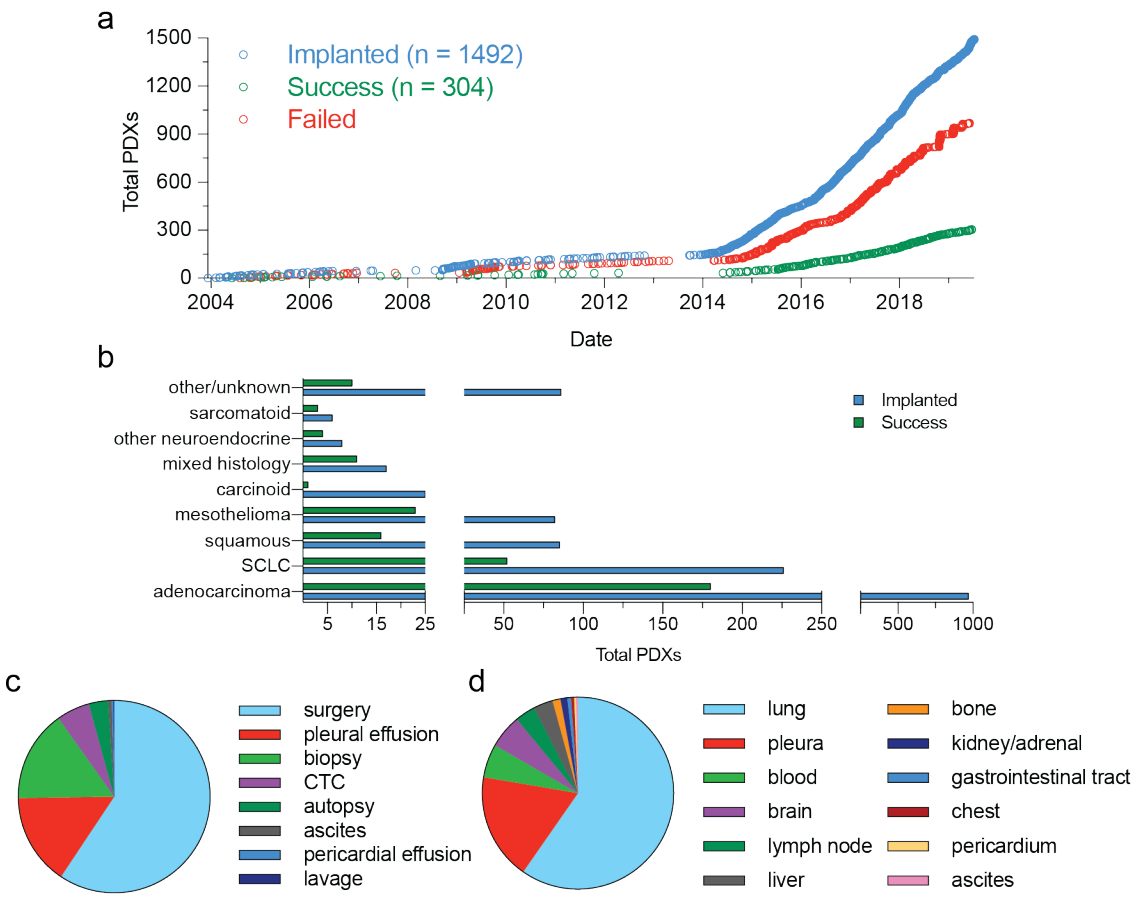

Figure 1.1. Development of a lung cancer PDX library
(a) Cumulative number of lung cancer PDXs implanted and successfully generated by the Rudin lab since 2004.
(b) Number of PDXs implanted and successfully generated for the indicated lung cancer subtypes.
(c) Percent of total PDX library implanted with cells from the indicated specimen type.
(d) Percent of total PDX library implanted with cells from the indicated tumor location.

CRISPR-Cas9

The discovery and characterization of CRISPR, led by numerous researchers over the last 25 years, has had an enormous impact on biological research (Lander, 2016). This is especially true in the field of cancer research, where there is a persistent need to understand the functional impact of genomic alterations observed in human tumors. Over the last 15 years, tumor sequencing efforts have detailed the immense scope of somatic mutations, copy number alterations, and genomic rearrangements present in diverse cancer types (Cancer Genome Atlas Research Network et al., 2013; Cheng et al., 2015). However, many of the genomic alterations identified are of unknown clinical significance and elucidating their role in cancer development and progression remains challenging (Chang et al., 2018). CRISPR has greatly expanded researchers' ability to perform functional genomic studies aimed at dissecting the biological impact of these genomic alterations.

The CRISPR system

Clustered regularly interspaced short palindromic repeats (CRISPR) is an RNA-guided adaptive immune system present in bacteria and archaea (Horvath and Barrangou, 2010). It was discovered when sequencing of prokaryotic genomes revealed a peculiar cluster of DNA repeats in many species, which were separated by unrelated spacer sequences and found near protein coding CRISPR-associated (Cas) genes with unknown function (Jansen et al., 2002; Mojica et al., 2000). An immune function for CRISPR was suggested when

analysis of the spacer sequences found homology to bacteriophages and other foreign DNA elements (Bolotin et al., 2005; Mojica et al., 2005; Pourcel et al., 2005) and this was later confirmed when it was observed that these sequences protected against phage infection with a matching sequence (Barrangou et al., 2007). Additional work showed that CRISPR elicited its function by targeting and cleaving DNA matching these spacer sequences (Garneau et al., 2010; Marraffini and Sontheimer, 2008), although RNA-targeting CRISPR-Cas systems have since been discovered (Abudayyeh et al., 2016).

CRISPR-Cas immunity occurs in three distinct stages, 1) adaptation to foreign DNA, 2) expression and processing of CRISPR RNAs, and 3) CRISPR interference (Marraffini and Sontheimer, 2010). During the adaptation phase, new spacer sequences, which are homologous to foreign DNA sequences called protospacers, are incorporated into the CRISPR array by the Cas1 and Cas2 proteins (Jackson et al., 2017). Protospacers are flanked by a conserved protospacer adjacent motif (PAM), which serves to prevent self-recognition and varies in sequence depending on the type of CRISPR system present (Deveau et al., 2008). To initiate CRISPR interference, the CRISPR array is transcribed as a single long precursor RNA that is subsequently processed into shorter CRISPR RNAs (crRNAs) containing a single spacer sequence. Some CRISPR systems utilize Cas proteins with endonuclease activity to process the pre-crRNA (Wang et al., 2011a), while other systems express a second RNA species called the trans-activating CRISPR RNA (tracrRNA) that directs RNase III to perform this digestion (Deltcheva et al., 2011).

In the final step of CRISPR-Cas immunity, crRNAs form a ribonucleoprotein (RNP) complex with effector Cas proteins to recognize and cleave foreign DNA (Marraffini and Sontheimer, 2010). Two broad classes of CRISPR systems (class I and class II) have been delineated based on the composition of this crRNA-effector complex. Class I systems utilize a multi-subunit effector complex whereas a single protein is used in class II systems (Makarova et al., 2015). Additionally, class II systems typically incorporate a tracrRNA into this complex (Shmakov et al., 2017). While taking different approaches, both classes of CRISPR systems result in sequence specific DNA cleavage of foreign DNA.

Genome engineering with CRISPR-Cas9

Genome engineering of mammalian cells largely relies on the creation of double-strand breaks (DSBs) at targeted genomic loci, which are subsequently repaired by one of two host cell DNA repair pathways to facilitate desired genomic alterations. The non-homologous end-joining (NHEJ) pathway is an error prone repair of DSBs that typically results in an insertion or deletion (indel) of genetic information. This can lead to frameshift mutations and gene disruption if it occurs in the protein coding region of a gene. Alternatively, the homology-directed repair (HDR) pathway precisely repairs DSBs by introducing a DNA repair template into the genomic locus through homologous recombination. Exogenous repair templates can be used to introduce specific point mutations or

insert large genomic fragments. Together, these DSB repair pathways enable a diverse range of genomic alterations in target cells (Hsu et al., 2014).

It was quickly appreciated that the bacterial CRISPR system might be an effective tool for creating DSBs in human cells with more flexibility than existing genome engineering methods (Barrangou, 2012; Carroll, 2012). To first adapt this system, *in vitro* reconstitution experiments demonstrated that the class II effector protein Cas9, crRNA, and tracrRNA were the minimum components necessary for DNA cleavage and, importantly, the crRNA and tracrRNA could be fused into a single-guide RNA (sgRNA) (Gasiunas et al., 2012; Jinek et al., 2012). Multiple groups then established that these components could be used to successfully edit the genome of human cells and the CRISPR revolution was off and running (Cong et al., 2013; Jinek et al., 2013; Mali et al., 2013b).

In addition to creating DSBs at specific genomic sites, engineered Cas9 variants have expanded the breadth of CRISPR-mediated genome engineering. While Cas9 “nickase" variants have been developed that create single strand DNA breaks rather than a DSB, the most useful Cas9 variant is the catalytically dead Cas9 (dCas9) that lacks nuclease activity (Jinek et al., 2012). dCas9 is able to bind to sequence-specific locations in the genome and, rather that creating a DSB, it acts as a scaffold for proteins with a diverse set of activities (Dominguez et al., 2016). These proteins can be a directly fused to dCas9 or are recruited to bind chimeric sgRNAs by the RNA binding protein MS2 (Mali et al., 2013a). Proteins utilized with dCas9 include transcriptional activators or repressors (Gilbert et al., 2014), fluorescent proteins (Chen et al., 2013),

epigenetic regulators (Hilton et al., 2015; Kearns et al., 2015; Liu et al., 2016b), and DNA base editors (Komor et al., 2016; Zafra et al., 2018). These Cas9 variants collectively expand the repertoire of CRISPR-mediated genome editing far beyond its initial discovery as an RNA-guided nuclease.

Inducible CRISPR-Cas9 systems

Temporal control of Cas9 activity in cancer models allows for genome editing at precise disease stages, such as in established xenograft tumors, and also limits off-target activity. Tetracycline (tet) (or interchangeably doxycycline (dox)) regulated gene expression is the most commonly used inducible system in mammalian cells. This system is based on a bacterial antibiotic resistance mechanism and consists of two components: 1) a tet-responsive protein, such as the tet-responsive repressor (TetR) or one of its many derivatives, and 2) a promoter containing a tet response element (TRE) (Das et al., 2016). Tet-responsive proteins can be classified as either Tet-On or Tet-Off systems based on whether they bind TRE in the presence or absence of tet, respectively. The reverse tet transcriptional activator (rtTA) is the most commonly used tet-responsive protein, which is a Tet-On protein that results in activated gene expression in the presence of dox (Gossen et al., 1995).

Since their discovery and characterization, tet regulated systems have been iteratively improved to enhance functionality. Several rtTA variants have been developed to increase dox-sensitivity and reduce background transcriptional activity of Tet-On systems. While the rtTA-V16 variant displays

the highest dox-sensitivity, it also has considerable background activity in the absence of dox (Zhou et al., 2006). Conversely, the rtTA-V10 variant was shown to have high activity and dox-sensitivity while also displaying minimal background transcriptional activity (Zhou et al., 2006). Additionally, TRE promoters used in Tet-On systems have been engineered to eliminate endogenous transcription factor binding sites that may otherwise activate transgene expression without rtTA binding. Of the variants tested, the TRE^{3GS} promoter was shown to have the lowest background transgene expression, yet a high dynamic range of induced expression (Loew et al., 2010).

Given that this system has been extensively characterized, several dox inducible CRISPR-Cas9 systems have been developed for regulating Cas9 expression in a variety of contexts, including genetically engineered mouse models (GEMMs) and cancer cell lines (Cao et al., 2016; Dow et al., 2015; González et al., 2014; Verma et al., 2017; Wang et al., 2014; Wu et al., 2018). Additionally, inducible sgRNA approaches have been developed that rely on dox regulation of RNA polymerase III promoters (Aubrey et al., 2015; Kiani et al., 2014), although these systems are less well characterized and expression can be highly variable (Dickins et al., 2005). Together, these systems demonstrate the feasibility of using dox to temporally control Cas9 activity, however, improved transcriptional control of Cas9 with optimized rtTA and TRE components could enhance the utility of these systems.

Alternative approaches to inducible Cas9 activity have relied on constitutive expression of engineered Cas9 variants that can be controlled post-

translationally by small molecule inducers. 4-hydroxytamoxifen (4-HT) can be used to control the nuclear localization of Cas9-ER fusions (Liu et al., 2016a; Oakes et al., 2016) or to regulate splicing of a Cas9-intein construct (Davis et al., 2015). Protein dimerization can be exploited for rapid activation of Cas9 constructs, either by using rapamycin to induce dimerization of a split Cas9 (Zetsche et al., 2015) or by disrupting the BCL-xL:BH3 inhibitory interaction in an engineered Cas9 (Rose et al., 2017). Protein destabilization domains have also been fused to Cas9 to enable post-translational control of Cas9 activity (Maji et al., 2017). While these constructs can be induced rapidly over short timeframes, these Cas9 variants invariably suffer from reduced or aberrant Cas9 activity and many of the chemical inducers elicit undesirable biological effects (Gangopadhyay et al., 2019).

CRISPR applications in cancer research

While there are too many applications to exhaustively list, several important CRISPR-Cas9 techniques have been used to elegantly model and dissect cancer phenotypes. Reproducing complex genetic events in GEMMs through somatic genome editing has been greatly enhanced by CRISPR-Cas9 and provides insights into how these genomic alterations affect tumor initiation, progression, and therapeutic response (Ventura and Dow, 2018). Somatic inactivation of tumor suppressors has been achieved in numerous mouse tissues using multiple Cas9 or sgRNA delivery methods, highlighting that this is an ideal platform for rapidly assessing how the inactivation of putative tumor suppressors

affects tumor development (Dow et al., 2015; Maresch et al., 2016; Sánchez-Rivera et al., 2014; Xue et al., 2014). Recurrent chromosomal rearrangements are a hallmark feature of many cancers that often result in oncogenic fusion proteins (Taki and Taniwaki, 2006). Historically, these events have been difficult to model; however, CRISPR has enabled the generation of complex genomic rearrangements through expression of two different sgRNAs targeting distant sites that comprise the fusion breakpoint (Blasco et al., 2014; Cook et al., 2017; Maddalo et al., 2014). Additionally, multiple groups have reported using CRISPR-Cas9 for the parallel generation of distinct point mutations at a single genomic locus using multiplexed HDR (Findlay et al., 2014; Winters et al., 2017). This allows simultaneous assessment of several precise genomic alterations in a single experiment and is rapidly scalable to include many genomic loci of interest. These GEMMs developed using CRISPR-Cas9 are valuable resources to model disease progression, assess therapeutic strategies, and interrogate the immune contexture of the tumor microenvironment.

In vitro cell line models are relatively easy to grow and manipulate; accordingly, it is now routine to perform single gene knockouts and other simple CRISPR-Cas9 experiments in these models. Nonetheless, these simple techniques can be used to answer complex cancer biological questions. CRISPR activation of SCLC subtype specific transcription factors in a precancerous cell line model was able to elucidate therapeutically actionable differences caused by expression of distinct transcription factors (Dammert et al., 2019). Moreover, DNA base editors are able to precisely edit genomic regions

with higher efficiency than HDR, and these are being used with both *in vitro* and *in vivo* models to recreate disease relevant mutations (Komor et al., 2016; Zafra et al., 2018). Another unique application is the rapid generation of drug resistance alleles created by tiling a protein domain with sgRNAs to produce a wide range of indels and then using drug selection to isolate novel resistance mutations (Ipsaro et al., 2017). Collectively, these experiments demonstrate the ability of simple CRISPR-Cas9 techniques to uncover novel aspects of complex cancer biology.

CRISPR screens allow for interrogation of complex cancer cell biology in sophisticated high throughput experiments (Doench, 2018). The first published CRISPR screens using gene knockout, transcriptional activation, or transcriptional repression demonstrated the feasibility of assessing phenotypes with a genome scale library (Gilbert et al., 2014; Shalem et al., 2014; Wang et al., 2014). Since, systematic screens in cell line panels have aimed to identify context specific vulnerabilities that could potentially be exploited by cancer therapeutics (Aguirre et al., 2016; Behan et al., 2019). Interestingly, it was observed that sgRNA libraries targeting functional protein domains could more robustly identify a loss of cellular fitness, as a higher fraction of generated mutations were deleterious (Shi et al., 2015). Recently, combinatorial screens with pairwise sgRNA libraries have endeavored to map the genetic interactions in cancer cells, with the hopes that previously unidentified interactions could be exploited to improve clinical outcomes (Han et al., 2017; Horlbeck et al., 2018). Increasingly, single cell RNA-sequencing platforms are being combined with

CRISPR screens to profile thousands of individual transcriptomes following genetic perturbation (Datlinger et al., 2017; Dixit et al., 2016; Norman et al., 2019). These techniques are collectively enabling the rapid interrogation of the entire genome's contributions to numerous cancer phenotypes.

Thesis Aims

PDXs are high fidelity *in vivo* tumor models that accurately reflect many key aspects of human cancer (Hidalgo et al., 2014). The hallmark feature of PDXs is that they are continuously passaged *in vivo*, which allows them to bypass the negative selective pressure imposed by *in vitro* growth (Daniel et al., 2009; Guo et al., 2016; Poirier et al., 2015). However, it is this continuous *in vivo* growth that precludes the use of PDXs with genome editing systems, as these largely rely on antibiotic selection methods that necessitate *in vitro* growth (Siolas and Hannon, 2013). As the genetic manipulation of cancer models is essential to understanding the functional significance of individual genes and variants to cancer biology (Ventura and Dow, 2018), this has severely limited the utility of PDXs in cancer research. In my thesis, I aim address this limitation by developing methods for performing CRISPR-Cas9 genome editing of PDXs using a tightly regulated, inducible Cas9 vector that does not require *in vitro* culture for selection of transduced cells.

In chapter 3 of my thesis, I aimed to develop a series of CRISPR-Cas9 vectors specifically for genetically manipulating PDXs. The main component of this platform is pSpCTRE, a dox-inducible Cas9 lentiviral vector with a $CD4^{T}$

selectable marker enabling rapid *ex vivo* selection of transduced cells. This vector is engineered for use in PDXs and includes a novel bidirectional promoter topology for the easy identification of cells that undergo Cas9-mediated genome editing. Additionally, I develop a flexible sgRNA reporter vector to track sgRNA populations in clonal competition assays and a rAAV vector that delivers an sgRNA and DNA repair template for performing precise genomic alterations via HDR.

In chapter 4 of my thesis, I demonstrate the utility of this platform to perform *in vivo* genome editing of PDXs. I generate a library of SpCTRE PDXs with dox-inducible expression of Cas9 and, using a clonal competition assay, analyze genetic dependencies of these models by targeted gene disruption. Additionally, I analyze mechanisms of acquired drug resistance by site-specific gene editing using templated homology-directed repair. These experiments validate that this *in vivo* genome editing platform is highly effective and substantially augments the utility of PDXs as genetically programmable models of human cancer.

CHAPTER 2

MATERIALS AND METHODS

Patient-derived xenografts (PDXs)

All animal experiments were approved by the Memorial Sloan Kettering Cancer Center (MSKCC) Animal Care and Use Committee. Primary tumors and whole blood samples collected for generation of PDX models were obtained with informed consent from patients under protocols approved by the MSKCC and Johns Hopkins institutional review boards. Subcutaneous flank tumors were generated as described previously (Gardner et al., 2017).

Cloning and plasmids

The plasmids generated in this study are available on Addgene as indicated. A list of all oligonucleotides used in this study is available in Table 2.1.

pSpCTRE (Addgene plasmid # 114010): EFS promoter expresses $CD4^{T}$-2A-rtTA-V10; TRE-3GS promoter controls tetracycline-inducible expression of *S.pyogenes* Cas9 as an all-in-one Tet-On system. This vector was derived from the pLVX-TetOne-Puro vector (Clontech), which was digested with XhoI and KpnI to remove the existing rtTA and Puro selection cassettes. The EFS-$CD4^{T}$-2A-rtTA-WPRE cassette was generated by gene synthesis (IDT) and inserted into the digested vector by Gibson assembly (NEB). Cas9 was PCR amplified

and inserted into the multiple cloning site by digestion with EcoRI and BamHI followed by overnight ligation with T4 ligase (NEB).

sgTrack-Gateway (Addgene plasmid # 114011), sgTrack-GFP (Addgene plasmid # 114012) and sgTrack-mCherry (Addgene plasmid # 114013): U6 promoter expresses a single sgRNA; EFS promoter upstream of the Gateway cassette expresses either TurboGFP or mCherry in the respective reporter vectors. These vectors are derived from lentiCRISPRv2 (Sanjana et al., 2014), wherein Cas9 was replaced by a Gateway cassette in-frame with the existing 2A-Puro by PCR amplification of the Gateway cassette and Gibson assembly into an XbaI and BamHI digested backbone. Gateway donor vectors with closed TurboGFP and mCherry cDNAs were used to generate the respective reporter vectors using LR clonase (Invitrogen) according to the manufacturer's protocol. sgRNAs were cloned into these vectors as previously described (Sanjana et al., 2014).

pAAV-GFP-sgHDR: pAAV-GFP was a gift from John T Gray (Addgene plasmid # 32395) (Gray and Zolotukhin, 2011). A synthetic DNA fragment comprising an SV40 polyA terminator, partial multiple cloning site (BglII, HindIII), the human U6 promoter, EGFR sgRNA, a 1.5 kb EGFR homology directed repair template containing the T790M mutation and destroying the sgEGFR PAM sequence, and a second partial multiple cloning site (ClaI, XhoI, XbaI) was cloned into the NotI and XbaI restriction enzyme sites of pAAV-GFP, replacing the original beta-globin polyA fragment. EGFR C797S coding and silent repair landmark mutations

were inserted via site directed mutagenesis using primer pair P1 to generate the rAAV vector.

lentiCas9-Blast (Addgene plasmid # 52962) and lentiGuide-Puro (Addgene plasmid # 52963) were gifts from Feng Zhang. pMD2.G (Addgene plasmid # 12259) and psPAX2 (Addgene plasmid # 12260) were gifts from Didier Trono. pLenti CMV Neo DEST (705-1) (Addgene plasmid # 17392) and pLenti CMV Puro (w118-1) (Addgene plasmid # 17452) were gifts from Eric Campeau and Paul Kaufman (Campeau et al., 2009). All Gateway recombination reactions were performed with BP clonase or LR clonase used according to the manufacturer's protocol (Invitrogen). TurboGFP cDNA was cloned into pLenti CMV Neo DEST (705-1). pDONR221/CD4 was purchased from DNASU (HsCD00413471). CD4ΔD$_{2\text{-}4}$;ΔIC linked to rtTA-V10 by a T2A sequence was generated by gene synthesis (IDT), Gateway adapted by PCR using primer pair P2, and cloned into pDONR221. CD4 domain D_2 was then added to this construct to generate CD4ΔD$_{3\text{-}4}$;ΔIC (CD4^{T}) by performing an outward PCR with primer pair P3, extracting domain D_2 from pDONR221/CD4 using primer pair P4 and performing a Gibson assembly (NEB) with the PCR products. All CD4 constructs were then cloned into pLenti CMV Puro (w118-1). sgRNAs were cloned into lentiGuide-Puro as previously described (Sanjana et al., 2014). All transformations were performed in One Shot Stbl3 Chemically Competent cells (Invitrogen). Plasmids were purified using QIAquick Spin Miniprep or Plasmid

Plus Midi kits (Qiagen) and digest verified prior to use. All PCRs were performed with Phusion High-Fidelity PCR Master Mix with HF Buffer (NEB).

sgRNA sequences

Target sequences for sgRNAs used in this study are available in Table 2.2.

Cell culture and lentivirus production

A549, PC9, and HEK239T cells were purchased from ATCC. A549 and PC9 cells were maintained in RPMI-1640 media supplemented with 10% Tet-Free FBS (Gemini) and 1x penicillin/streptomycin (pen/strep, Gibco) and HEK239T cells were maintained in DMEM media supplemented with 10% FBS (Gemini) and 1x pen/strep. All cell lines were verified negative for mycoplasma within 6 months of use. Lentivirus was produced by transfecting HEK293T cells with a 3:2:1 ratio of lentiviral plasmid:psPAX2:pMD2.G with JetPrime transfection reagent (Polyplus) at a 2:1 JetPrime:DNA ratio. Media was changed 24 h after transfection and viral supernatants were collected 72 h after transfection. Viral supernatants were syringe filtered with a 0.45 uM PVDF filter (Millipore) and concentrated approximately 20 fold with Lenti-X Concentrator (Clontech) according to the manufacturer's protocol. All lentivirus was titered in A549 cells to control for batch-to-batch variability and to normalize titers between different lentiviral backbones. *In vitro* lentiviral transductions were performed with 8 μg/mL hexadimethrine bromide (polybrene, Sigma) and at a multiplicity of infection (MOI) of approximately 1, unless otherwise stated.

In vitro validation of pSpCTRE

An A549^{GFP} cell line containing a stably integrated, single-copy TurboGFP gene was generated by transducing A549 with pLenti CMV Neo/TurboGFP lentivirus (MOI 0.3) and single cell FACS sorting using a FACSAria (BD Biosciences). A549^{GFP} cells were subsequently transduced with lentiCas9-Blast or pSpCTRE lentivirus (MOI 0.3) and selected with blasticidin or CD4^{T} single cell FACS sorting, respectively, to generate stable A549^{GFP} Cas9 cell lines. A549^{GFP} Cas9 cells were transduced with lentiGuide-Puro/sgGFP or sgNTC lentivirus and selected with puromycin for 3 days. For analysis of GFP editing efficiency and dox dose response of pSpCTRE, 1 x 10^5 cells were plated in a 10 cm plate and treated with 0.5 µg/mL doxycycline (dox, Sigma) or a dox dose range, respectively, for 10 days. Cell pellets were collected to perform Western blot, Tracking of Indels by Decomposition (TIDE), or flow cytometry analysis as described below. To screen for Cas9 editing in the absence of dox, A549^{GFP}-SpCTRE cells with lentiGuide-Puro/sgGFP were maintained in culture for 6 weeks in RPMI with tet-free FBS. Cells were split when they reached approximately 70% confluence and flow cytometry analysis was performed every 7 days as described below. At day 35, cells not previously treated with dox were split and 0.5 µg/mL dox was added to half of the cells (crossover). *In vitro* competition assays were performed in A549 cells transduced with lentiCas9-Blast or pSpCTRE lentivirus (MOI 0.3) and selected with blasticidin or CD4^{T} single cell FACS sorting, respectively. A549 Cas9 cell lines were independently transduced with sgTrack lentivirus and, after 3 days, cells containing control and

test sgRNAs were mixed with an equal ratio of GFP and mCherry positive cells. Cells were split and flow analysis was performed as described below every 4 days. Results for all experiments represent three independent biological replicates.

Antibodies

A list of antibodies used in this study is available in Table 2.3.

Protein extraction, Western blotting and LiCor protein quantification

Whole cell lysates were prepared from frozen cell pellets or flash frozen tumor samples using RIPA lysis buffer with 1x HALT protease inhibitor cocktail (Thermo). Cell pellets were resuspended in 5 volumes of cold lysis buffer and incubated on ice for 10 minutes, followed by sonication for 10 seconds with a 200V microtip sonicator set to 40% amplitude (QSonica, CL 18). Lysates were clarified by centrifugation at 20,000 x g for 10 minutes at 4C. Protein extraction from flash frozen tumor samples was performed as previously described (Gardner et al., 2017). Protein was quantified using a BCA protein assay kit (Pierce) and samples were denatured at 70C for 10 minutes in NuPAGE LDS sample buffer with NuPAGE sample reducing agent and then resolved on a 4-12% Bis-Tris gradient gel (Invitrogen). For chemiluminescent detection, gels were wet-transferred to 0.45 μm Immobilon-P PVDF membrane (Millipore) and incubated overnight at 4C with primary antibody diluted in TBS (Fisher) supplemented with 0.1% Tween20 (Fisher) and either 5% BSA (Cell Signaling) or

5% non-fat dry milk (Oxoid). Blots were then incubated at room temperature for 1 hour with the relevant secondary antibody diluted in TBS supplemented with 0.1% Tween20 and 5% non-fat dry milk and then detected using ECL Western Blotting Substrate (Pierce). Protein transfer, detection, and quantification using LiCor was performed as previously described (Gardner et al., 2017).

Tracing of Indels by Decomposition (TIDE) analysis

Genomic DNA was extracted from cell pellets using the DNeasy Blood & Tissue kit (Qiagen). An approximately 800-bp region centered on the sgRNA cut site was PCR amplified from 50 ng of genomic DNA using primer pair P5 (sgGFP) or P6 (sgRPA1-1) (Table 2.1). Completed PCR reactions were treated with exonuclease I (NEB) according to the manufacturer's protocol and then purified with the QIAquick PCR purification kit (Qiagen). 20 ng of purified PCR product was Sanger sequenced using an M13-forward primer and chromatograms were analyzed as previously described (Brinkman et al., 2014).

Flow cytometry analysis for *in vitro* experiments

A549-SpCTRE or A549^{GFP}-SpCTRE cells for flow cytometry analysis were collected using TrypLE Express (Thermo) according to the manufacturer's protocol to preserve CD4^{T} cell surface expression. Approximately 1 million cells were resuspended in PBS containing human TruStain FcX (Biolegend) and incubated at 4C for 10 minutes. Cells were stained with the α-CD4 antibody for 30 minutes at 4C, then washed twice with PBS and resuspended in PBS

containing 1 μg/mL DAPI. All α-CD4 staining was performed with PE anti-human CD4 antibody clone RPA-T4 (Biolegend), unless otherwise stated. For analysis of GFP expression in CD4 negative cells (i.e. $A549^{GFP}$-lentiCas9-Blast), approximately 1 million cells were washed twice with PBS and resuspended in PBS containing 1 μg/mL DAPI. All flow analysis was performed on an LSR Fortessa or LSR II (BD Biosciences).

$CD4^T$ extracellular domain analysis

A549 cells were co-transfected with a 50:50 mix of each CD4 domain variant and pLenti Neo CMV/TurboGFP using JetPrime transfection reagent (Polyplus) at a 2:1 JetPrime:DNA ratio. Media was changed 24 h after transfection and cells were selected with puromycin for 3 days. Flow cytometry analysis was performed as described above with PE anti-human CD4 antibody clones M-T466 (Miltenyi), RPA-T4, SK3, and OKT4 (Biolegend). Mean fluorescence intensity (MFI) of GFP positive cells was calculated using FlowJo. To compare antibody binding between $CD4^T$ and full-length CD4, A549 was transduced with pLenti CMV Puro/CD4 lentivirus and selected with puromycin for 3 days. This cell lines was mixed with $A549^{GFP}$-SpCTRE and flow cytometry analysis was performed as described above using anti-human CD4 antibodies RPA-T4 (APC) and OKT4 (PE).

Magnetic cell separation (MACS)

A549-SpCTRE cells were spiked into an $A549^{GFP}$ cell suspension at an abundance of 5-20%. This mixture was incubated with CD4-APC antibody (Miltenyi) and anti-APC microbeads (Miltenyi) and subjected to magnetic separation with LS columns (Miltenyi) according to the manufacturer's protocol. Eluted cells were cultured for 3 days to allow for dissociation of magnetic beads and then collected for flow cytometry analysis of $CD4^{T}$ purity, as described above. Results represent three independent biological replicates. To isolate $CD4^{T}$ induced cells, CD4 microbeads (Miltenyi) were used according to the manufacturer's protocol.

Transduction and enrichment of SpCTRE PDXs

Established PDX tumors were resected and dissociated to a single cell suspension using a gentleMACS tissue dissociator with a human tumor dissociation kit (Miltenyi). Red blood cells were lysed with ACK lysing buffer (Lonza) and mouse stroma cells were subsequently removed by negative magnetic bead selection using a mouse cell depletion kit (Miltenyi). Cells were then transduced *ex vivo* with pSpCTRE lentivirus at a relative MOI of 1-6 (based on a functional titer performed in A549) in the presence of 48 µg/mL polybrene in a swinging bucket rotor for 30 min at 800 x g. After transduction, cells were washed twice with PBS to remove the lentivirus and polybrene and engrafted in a 50% Matrigel (BD) mixture into a single flank of 6-8 week old NSG (Jax) or Nude (Envigo) mice. Resulting tumors were dissociated to a single cell suspension,

red blood cells were lysed, and mouse stroma was removed as described above. Cells were prepared for flow cytometry sorting or analysis by resuspending 5-10 million cells (sorting) or 1 million cells (analysis) in FACS buffer (PBS with 2% FBS, 1X pen/strep and 1 mM EDTA) containing human TruStain FcX (Biolegend) and mouse TruStain FcX (anti-mouse CD16/32, Biolegend) and incubating at 4C for 10 minutes. Cells were stained with APC/Cy7 anti-human CD4 (clone RPA-T4, Biolegend) and AlexaFluor647 anti-mouse H-2K^{d} (clone SF1-1.1, Biolegend) for 30 minutes at 4C. Cells were washed twice with MACS buffer (PBS with 0.5% BSA) and then resuspended in sorting buffer (PBS with 0.5% BSA, 2.5 mM $MgCl_2$, 0.5 mM $CaCl_2$, 1 µg/mL DAPI and 100 U/mL DNaseI, NEB) and incubated for 30 minutes at room temperature before sorting. CD4^{T} positive, H-2K^{d} negative, DAPI negative cells were collected using a FACSAria (BD Biosciences) and engrafted in a 50% Matrigel mixture into a single flank of a 6-8 week old NSG or Nude mouse. Resulting tumors were collected and analyzed for CD4^{T} expression as described above. If the tumor was less than 50% CD4^{T} positive, it was sorted again as described and if the tumor was >=50% CD4^{T} positive it was propagated or cryo preserved in RPMI supplemented with 10% FBS, 1x pen/strep, and 10% DMSO. SNP profiles of SpCTRE PDXs were compared to pre-sorted samples using qPCR genotyping of 8 informative SNPs to confirm identity.

In vivo competition assays in SpCTRE PDXs

Established SpCTRE PDX tumors were dissociated to a single cell suspension, red blood cells were lysed, and mouse stroma was removed as described above. Cells were then independently transduced *ex vivo* with sgTrack lentivirus at a relative MOI of 1 as described above. Each sgTrack transduced SpCTRE PDX was engrafted in a 50% Matrigel mixture into a single flank of a 6-8 week old NSG or Nude mouse. Resulting tumors were dissociated to a single cell suspension, red blood cells were lysed, and mouse stroma was removed as described above. Cells containing control and test sgRNAs were mixed with an equal ratio of GFP and mCherry positive cells and engrafted in a 50% Matrigel mixture into a single flank of 6-8 week old NSG or Nude mice. Once tumors reached ~100 mm^3, mice were randomized to control or dox-treated groups, with dox-treated mice receiving 625 mg/kg doxycycline chow (Envigo). Tumors were collected once they reached 1000 mm^3, dissociated to a single cell suspension, and prepared for flow cytometry analysis or sorting as described above. Indel analysis of sorted cells was performed as described above and fitness scores and log ratios were calculated as described in Figure 3.7. The Wilcoxon rank sum statistic was used to test if the fitness scores in the dox-treated group were smaller than the fitness scores in the control group.

Recombinant AAV production and validation

Recombinant AAV2/6 pseudotyped virus was produced by the Boston Children's Hospital Viral Core. PC9 cells transduced with lentiCas9-Blast and selected with

blasticidin for 7 days were subsequently transduced with rAAV at an MOI of 2.3. Control and rAAV transduced PC9-lentiCas9-Blast cells were treated with 1 μM osimertinib (Selleck Chemicals) or DMSO (Corning) until they reached confluency, at which time cell pellets were collected for genomic analysis, described below. Osimertinib resistance was confirmed in cells previously transduced with rAAV and selected with osimertinib by seeding 3000 viable cells per well in 100 μL/well media containing a dilution series of osimertinib. Viability was assayed 72 h after plating using CellTiter-Glo (Promega).

In vivo homology-directed repair in MSK-LX29

Crizotinib (LC Laboratories), osimertinib (LC Laboratories), or the combination were formulated in 0.5% hydroxypropyl methylcellulose (HPMC) and given by oral gavage at 25 mg/kg daily for 5 days per week. An MSK-LX29-SpCTRE tumor from a mouse fed with dox chow for 4 weeks prior to dissociation was incubated with the rAAV at an MOI of 1.6 million genomic copies/cell for 1 hour at 37C. Cells were washed twice with PBS and then engrafted in a 50% Matrigel mixture in the flank of 6-8 week old NSG mice. All mice were administered dox chow at the time of engraftment and treatment groups were randomized once tumors reached 100 mm^3. Tumors were collected once they reached 1000-1500 mm^3 and genomic analysis was performed as described below.

Genomic analysis of EGFR homology-directed repair

Genomic DNA was purified from dissociated tumors or cell pellets using the

Gentra Puregene Cell kit (Qiagen). A 1,122 bp amplicon, which spans outside the rAAV homology arms to ensure amplification occurs from genomic DNA, was PCR amplified from 200 µg genomic DNA using primer pair P7. The PCR product was then digested with exonuclease I to remove excess primers, column purified using the QIAquick PCR purification kit (Qiagen), and 100 µg was used as the template for a second PCR with primer pair P8 to amplify a 273 bp region centered on the repair site. The second round PCR product was column purified and paired-end Next-Gen sequencing (NGS) was performed by the CCIB DNA Core Facility at Massachusetts General Hospital (Cambridge, MA). NGS sequencing was analyzed using the R statistical computing environment to determine the proportion of reads that underwent rAAV-mediated homology-directed repair.

Table 2.1. List of oligonucleotides used in this study

Primer pair	Gene	Forward (5' to 3')	Reverse (5' to 3')	Purpose
P1	-	CATGCCCTTCG GCTCACTCCTG GACTATG	CATAGTCCAGG AGTGAGCCGAA GGGCATG	Mutagenesis of T790M rAAV repair template to produce T790M/C797S repair template
P2	-	GGGGACAAGTT TGTACAAAAAA GCAGGCTTAAT GAACCGGGGAG TCCCTTTTAGG	GGGGACCACTT TGTACAAGAAA GCTGGGTATTA CCCGGGGAGC ATGTCAAGGTC	Gateway adapt CD4ΔD2-4;ΔIC - T2A - rtTA-V10
P3	-	TCTGGCGGTGG ATCCGGAATGG	CAATCCGAACA CTAGCAATTGC ACCTC	Outward PCR to insert CD4 domain D2 between domain D1 and transmembrane domain
P4	-	GAGGTGCAATT GCTAGTGTTCG GATTG	AATCAGGGCCA TTCCGGATCCA CCGCCAGAAGC TAGCACCACGA TGTCTATTTTGA AC	Extract CD4 domain D2 for Gibson assembly to generate CD4ΔD3-4;ΔIC ($CD4^T$)
P5	Turbo GFP	GTAAAACGACG GCCAGCACCAA AATCAACGGGA CTT	CAGGAAACAGC TATGACCTTGA AGTGCATGTGG CTGT	Indel analysis of sgGFP
P6	RPA1	GTAAAACGACG GCCAGGGGGTC AGCTGCCCTAT ACT	CAGGAAACAGC TATGACGCAAA ACCCCGTTTCT ACC	Indel analysis of sgRPA1-1
P7	EGFR	TGCTAGGTCTTT TGCAGGCA	GCCTGCCTGCA AATCCTTTA	Round 1 PCR for NGS analysis of EGFR HDR
P8	EGFR	CCAGGAAGCCT ACGTGATGG	CTCTTGCTATC CCAGGAGCG	Round 2 PCR for NGS analysis of EGFR HDR

Table 2.2. List of sgRNA sequences used in this study

sgRNA	Target	Target sequence	Source
sgGFP	TurboGFP	CTGCACGCCATCAACAACGG	original
sgNTC	Nontargeting	ACGGAGGCTAAGCGTCGCAA	(Shalem et al., 2014)
sgRPA1-1	RPA1	GACACAGTTGAACCCTCTCG	(Wang et al., 2015)
sgRPA1-2	RPA1	CGTACCTGGAGCAACTCCCG	(Wang et al., 2015)
sgKRAS-1	KRAS	AGAGGAGTACAGTGCAATGA	(Doench et al., 2016)
sgKRAS-2	KRAS	CGAATATGATCCAACAATAG	(Doench et al., 2016)
sgEGFR	EGFR	CTGCGTGATGAGCTGCACGG	original

Table 2.3. List of antibodies used in this study

Target	Used to detect	Supplier	Product #	Fold dilution
β-actin	-	Cell Signaling	4967	10,000
Cas9	-	Active Motif	91123	1,000
TurboGFP	-	Pierce	PA5-22688	5,000
Vinculin	-	Cell Signaling	13901	10,000
Anti-2A peptide	$CD4^T$	Millipore	ABS31	2,000
TetR	rtTA	Clontech	631131	1,000
EGFR	-	Cell Signaling	2232	1,000
p-EGFR	-	Cell Signaling	2234	1,000
MET	-	Cell Signaling	8198	1,000
p-MET	-	Cell Signaling	3077	1,000
ERK	-	Cell Signaling	9102	1,000
p-ERK	-	Cell Signaling	4370	1,000
p-S6	-	Cell Signaling	4857	1,000
Anti-rabbit IgG, HRP-linked	-	Cell Signaling	7074	3,000
Anti-mouse IgG, HRP-linked	-	Cell Signaling	7076	3,000
IRDye 680LT donkey anti-rabbit IgG	-	LICOR	926-68023	25,000
IRDye 800CW donkey anti-mouse IgG	-	LICOR	926-32212	25,000

CHAPTER 3

Design and validation of a CRISPR-Cas9 platform tailored for use in PDXs

Introduction

The ability to genetically manipulate cancer models has played an essential role in defining the functional contributions of individual genes and variants to cancer biology and CRISPR-Cas9 has greatly expanded our ability to rapidly perform these studies (Sánchez-Rivera and Jacks, 2015; Ventura and Dow, 2018). CRISPR-Cas9 can be used to disrupt genes through the introduction of frameshift insertions and deletions (indels) by non-homologous end joining (NHEJ) or to precisely alter genomic sequences through homology-directed repair (HDR) (Komor et al., 2017). Combining this technology with *in vivo* cancer models provides a platform on which to study carcinogenesis and tumor maintenance in a complex environment resembling that of human tumors (Ventura and Dow, 2018).

A diverse array of CRISPR-Cas9 systems have been developed in recent years to perform genome editing of cancer models (Tschaharganeh et al., 2016). Despite the proven utility of PDXs, application of these systems to *in vivo* cancer models has been restricted to xenografts of established human and mouse cell lines cultured extensively *in vitro* or genetically engineered mouse models (GEMMs) (Sánchez-Rivera and Jacks, 2015; Ventura and Dow, 2018). The continuous *in vivo* passaging of PDXs precludes the use of antibiotic selection

methods extensively employed by current CRISPR-Cas9 systems (Siolas and Hannon, 2013). While CRISPR-Cas9 vectors with alternative selection methods have been developed (Ablain et al., 2015; Kabadi et al., 2014; Meca-Cortés et al., 2017), they all lack the complete set of features requisite for use in PDXs, namely 1) a selection strategy applicable in these models, 2) a lentiviral vector with optimized titer, and 3) tightly regulated temporal control of Cas9 expression.

Tight temporal control of Cas9 activity is especially critical for *in vivo* tumor studies to validate genes required for tumor maintenance and to credential suppressor mutations that may play a role in acquired drug resistance (Dow et al., 2015; 2014). Several inducible systems have been developed to regulate Cas9 activity at the post-translational level, yet these systems invariably suffer from aberrant or reduced Cas9 activity [reviewed by (Gangopadhyay et al., 2019)]. Doxycycline (dox)-inducible expression of Cas9 provides a combination of maximum cutting efficiency in the "on" state while minimizing Cas9 activity in the "off" state through tight transcriptional regulation. However, many current systems are reported to lack complete transcriptional control by dox and are not amenable for use in PDXs because they either rely on inefficient knock-in approaches (Dow et al., 2015; González et al., 2014; Wu et al., 2018) or employ vectors that exceed the lentiviral packaging limit and consequently result in low viral titers and predictably poor transduction efficiency (Cao et al., 2016; Verma et al., 2017). These limitations have precluded the application of existing genome editing systems to PDXs. Given the increasingly central role of PDXs in cancer research, a technological advance to enable inducible CRISPR-Cas9

genome editing of these models would have broad utility to further our understanding of cancer biology and facilitate the development of new therapeutic strategies.

In this chapter, we develop a platform for performing CRISPR-Cas9 genome editing in PDXs and validate the utility of this platform using *in vitro* models. The key component of this system is pSpCTRE, an all-in-one dox-inducible Cas9 lentiviral vector designed specifically for use in PDXs. This vector encodes a truncated CD4 selection marker engineered to be minimal in size yet able to facilitate rapid antibody-based selection of pSpCTRE-transduced cells. A unique promoter topology employed in pSpCTRE creates a novel cell surface marker of Cas9 expression and genome editing produced by bidirectional promoter induction. Additionally, two sgRNA expression vectors were developed for use in combination with pSpCTRE for *in vivo* functional genomic applications. First, sgTrack pairs sgRNA expression with a series of reporter constructs that can be quickly and easily interchanged to interrogate genetic dependencies in PDXs through internally controlled clonal competition assays. Second, we developed a recombinant AAV vector (rAAV) to simultaneously deliver an sgRNA and DNA repair template for performing precise genomic alterations via homology-directed repair. The vectors developed herein are the first to be targeted specifically for use in PDXs and enable a wide range of functional genomic applications in these cancer models.

Results

pSpCTRE: an inducible Cas9 vector tailored for use in PDXs

pSpCTRE (*Streptococcus pyogenes* Cas9 – Tet Response Element) is an all-in-one dox-inducible Cas9 lentiviral vector tailored for use in PDXs (Fig. 3.1a). A novel, constitutively expressed truncated CD4 (hereafter $CD4^T$) selectable marker enables rapid, positive selection of pSpCTRE-transduced cells without prolonged *in vitro* culture, allowing the system to be employed with PDXs (Fig. 3.1b). Selectable cell surface markers are particularly useful as they can be enriched through rapid and relatively benign methods such as fluorescence activated cell sorting (FACS) or magnetic bead selection (Bonini et al., 1997; Gaines and Wojchowski, 1999). The diverse range of commercial α-CD4 reagents ensures the availability of bright fluorophores that are spectrally compatible with fluorescent protein markers used in downstream applications. $CD4^T$ is a compatible selectable marker for PDXs as immunodeficient mice lack endogenous lymphocytes that may interact with tumor-expressed CD4 (Hirenallur-Shanthappa et al., 2016) and $CD4^T$ lacks the cytoplasmic domain of CD4 required for signal transduction (Koretzky, 2010).

We designed pSpCTRE to achieve tight temporal control of Cas9 activity and sensitive induction through extensive optimization of its substituent components. The TRE^{3GS} promoter is engineered to eliminate endogenous transcription factor binding sites thereby minimizing leaky Cas9 expression in the absence of dox (Loew et al., 2010), while the rtTA-V10 variant used displays

increased sensitivity to low dox concentrations and may improve inducibility *in vivo* (Zhou et al., 2006). Additionally, several studies have shown that relative genome editing efficiency is strongly correlated with Cas9 protein expression, where poorly expressed constructs demonstrate poor editing efficiency (Kim et al., 2017; Zafra et al., 2018). Therefore, it is imperative to employ an inducible system that can drive sufficient expression of Cas9. To this end, the reverse promoter orientation used in pSpCTRE has been shown to produce significantly higher levels of transgene expression than a similar construct with a forward promoter orientation (Heinz et al., 2011). Together, these design features of pSpCTRE create a tightly regulated system capable of responding to low dox concentrations and expressing sufficiently high amounts of Cas9 to produce efficient genome editing.

An added challenge in the design of pSpCTRE is creating a system with all of the necessary components to inducibly express Cas9 yet adequate lentiviral titer to successfully transduce PDXs. Lentiviral titer decreases as a function of proviral size (Kumar et al., 2001) and the relatively large size of Cas9 has made it challenging to develop high titer systems in the past (González et al., 2014; Sanjana et al., 2014). For this reason, several approaches were explored to reduce the overall size of pSpCTRE or add vector elements aimed at increasing titer. The optimal composition of $CD4^{T}$ was empirically determined through a deletion series of the extracellular Ig-like domains to find the minimum domain structure required for binding of commercial α-CD4 antibodies (Fig. 3.2a). While several α-CD4 antibody epitopes reside within domain D_1 (Helling et al.,

2015), we found that both domains D_1 and D_2 were required for binding by these antibodies. Based on this finding, $CD4^T$ is composed of the CD4 signal peptide and extracellular domains D_1 and D_2 fused to the transmembrane domain (TM) via a flexible linker, with D_3, D_4, and the intracellular portion of the protein omitted entirely. The final coding sequence is approximately half the size of full-length CD4 and can be used with commercial flow cytometry or magnetic bead sorting reagents (Fig. 3.2b, c). To further minimize vector size, we use the minimal EFS promoter to drive constitutive expression of the CD4 selectable marker and rtTA-V10, which are joined by a T2A self-cleaving peptide.

Finally, we explored adding lentiviral elements to pSpCTRE that are reported to increase viral titer, specifically a woodchuck hepatitis virus post-transcriptional regulatory element (WPRE) and a second central polypurine tract (cPPT). The WPRE increases RNA stability and is reported to increase both transgene expression and lentiviral titer (Brun et al., 2003), while the cPPT facilitates nuclear export of the lentiviral RNA for packaging (Logan et al., 2004). While adding to the overall size of the vector, addition of a WPRE to the 3' end of the vector dramatically increased titer, however, an additional cPPT sequence between the two promoters had no effect (Fig. 3.3). Since pSpCTRE already included one cPPT, its possible that this alone was sufficient for nuclear export of the viral RNA. These optimizations collectively result in a final pSpCTRE size of 9,023 bp between the LTRs and maximized lentiviral titer.

In addition to reducing vector size, the truncated $CD4^T$ allows pSpCTRE to be used in the context of CD4-expressing cells, as the former lacks extracellular

domains D_3 and D_4. Therefore, $CD4^T$ can be distinguished from full-length CD4 by staining with both domain D_1 and D_3 specific antibodies (Fig. 3.4a). Cells with full length CD4 will stain with both antibodies and can be easily identified as a double positive population, whereas the cells with $CD4^T$ are single positive (Fig. 3.4b-d).

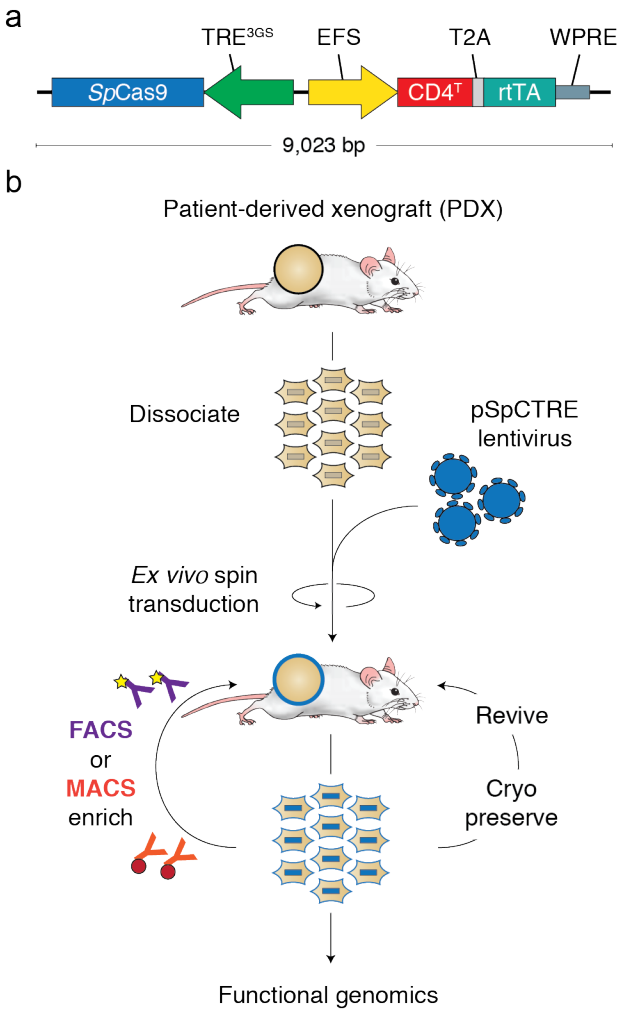

Figure 3.1. pSpCTRE for dox-inducible Cas9 expression in PDXs
(a) Vector map. $CD4^T$ is a minimal, truncated CD4 selectable marker linked to rtTA-V10 by a T2A ribosome skipping sequence that enables pSpCTRE to be used with PDXs (see **Fig. 3.2** for $CD4^T$ details).
(b) Schematic of Cas9 PDX generation. Dissociated tumors are transduced *ex vivo* with pSpCTRE lentivirus and immediately engrafted in mice without intervening *in vitro* culture. Resultant SpCTRE PDXs (blue outline) are then subjected to CD4 enrichment, cryopreservation, or functional studies.

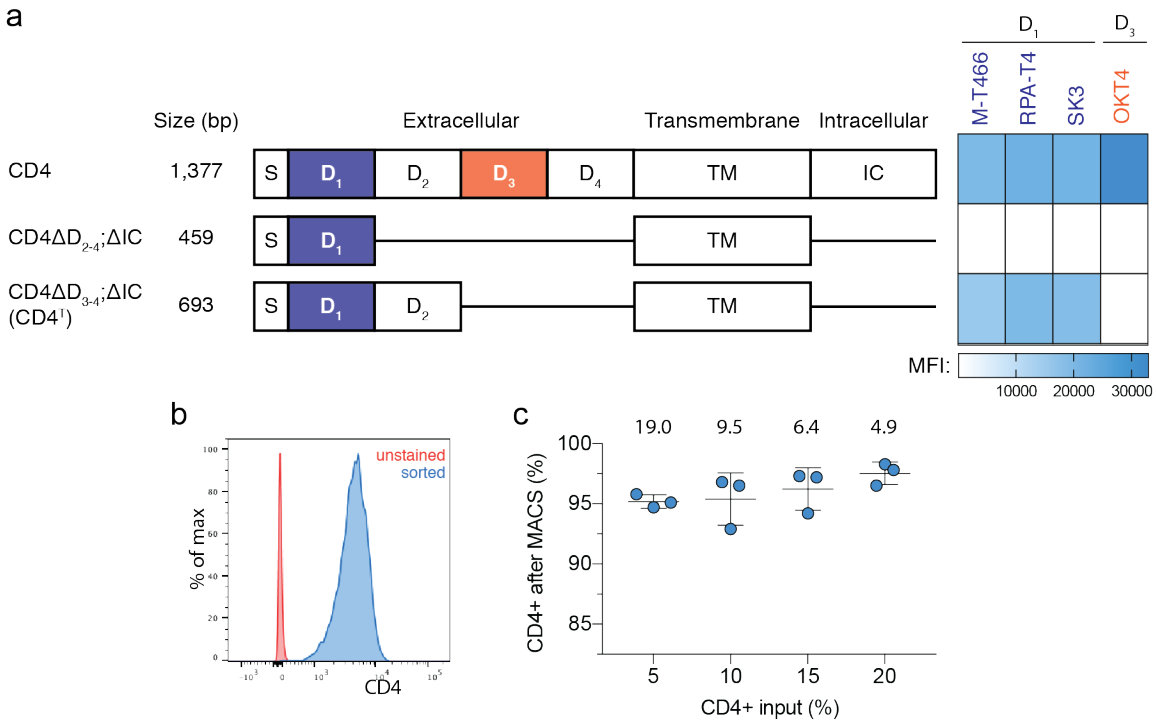

Figure 3.2. Truncated CD4^T is a size efficient selectable marker for flow cytometry and magnetic bead selection

(a) Domain structure of wildtype human CD4 and truncated constructs CD4ΔD$_{2-4}$;ΔIC and CD4ΔD$_{3-4}$;ΔIC (CD4^T), where the indicated deletions are replaced by flexible linkers. Heatmap depicts flow cytometry staining intensity of commercially available α-CD4 antibodies, which target the indicated extracellular domains of CD4, to the indicated CD4 constructs. S, signal peptide; TM, transmembrane domain; IC, intracellular domain; MFI, mean fluorescence intensity.

(b) Flow cytometry analysis of A549 cells expressing CD4^T and enriched by fluorescence activated cell sorting (FACS).

(c) Magnetic bead enrichment of A549 cells expressing CD4^T, with the indicated enrichment factors (above). Error bars are SD (n = 3).

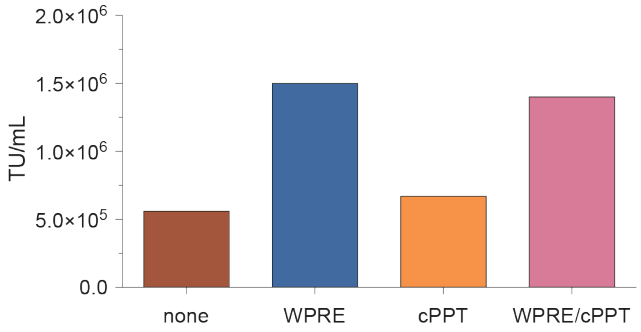

Figure 3.3. Analysis of lentiviral titer with addition of WPRE or cPPT elements
Lentiviral titer was analyzed for pSpCTRE variants containing the indicated vector elements.

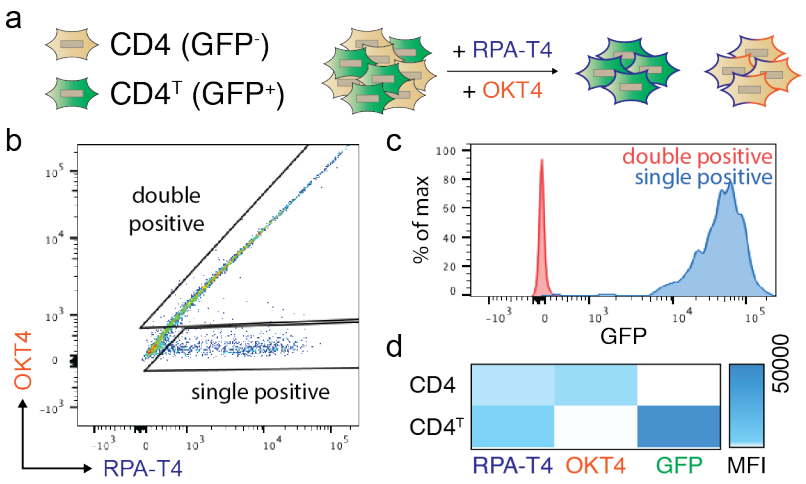

Figure 3.4. α-CD4 staining strategy with domain D_1 and D_3 targeting antibodies to differentiate $CD4^T$ and full-length CD4 using flow cytometry
(a) Experiment schematic. A mixture of GFP-negative cells expressing full length CD4 and GFP-positive cells expressing $CD4^T$ were stained with the indicated α-CD4 antibody clones and distinguished based on α-CD4 single or double positivity.
(b) CD4 surface expression as determined by α-CD4 antibody clones RPA-T4 (D_1) and OKT4 (D_3).
(c) GFP expression for cells gated based on α-CD4 single or double positivity as determined in (b).
(d) Heat map summarizing flow cytometry data in (b) and (c).

pSpCTRE gene editing is tightly regulated by doxycycline

We validated pSpCTRE design elements discussed in the previous section through *in vitro* disruption of GFP in A549 cells expressing GFP ($A549^{GFP}$). First, we examined the editing efficiency of pSpCTRE compared to constitutively expressed Cas9 to determine if pSpCTRE can express sufficient levels of Cas9 to efficiently edit cells. In the absence of dox, $A549^{GFP}$-SpCTRE cells transduced with sgGFP maintained GFP expression and had no detectable Cas9 protein by Western blot (Fig. 3.5a, b). Conversely, after exposure to dox, $A549^{GFP}$-SpCTRE cells edited GFP with similar efficiency to $A549^{GFP}$ cells constitutively expressing Cas9 from the lentiCas9-Blast vector (Fig. 3.5a, b). We observed a dose-dependent increase in Cas9 expression with concomitant loss of GFP expression with as little as 0.0625 μg/mL dox and a maximum loss of GFP expression at 0.25 μg/mL dox, defining an upper and lower bound for dox response (Fig. 3.5c).

To more sensitively screen for leaky expression of Cas9 and undesired genome editing, we cultured $A549^{GFP}$-SpCTRE cells transduced with sgGFP in the absence of dox. We observed no decrease in GFP-positive cells over >10 passages. However, these cells retained the capacity to efficiently disrupt GFP upon dox induction after 35 days of continuous culture, conditions that mimic dox-induction in established tumors (Fig. 3.5d). These data indicate that pSpCTRE is a tightly regulated dox-inducible Cas9 vector that meets our requirements for *in vivo* use in PDX tumors.

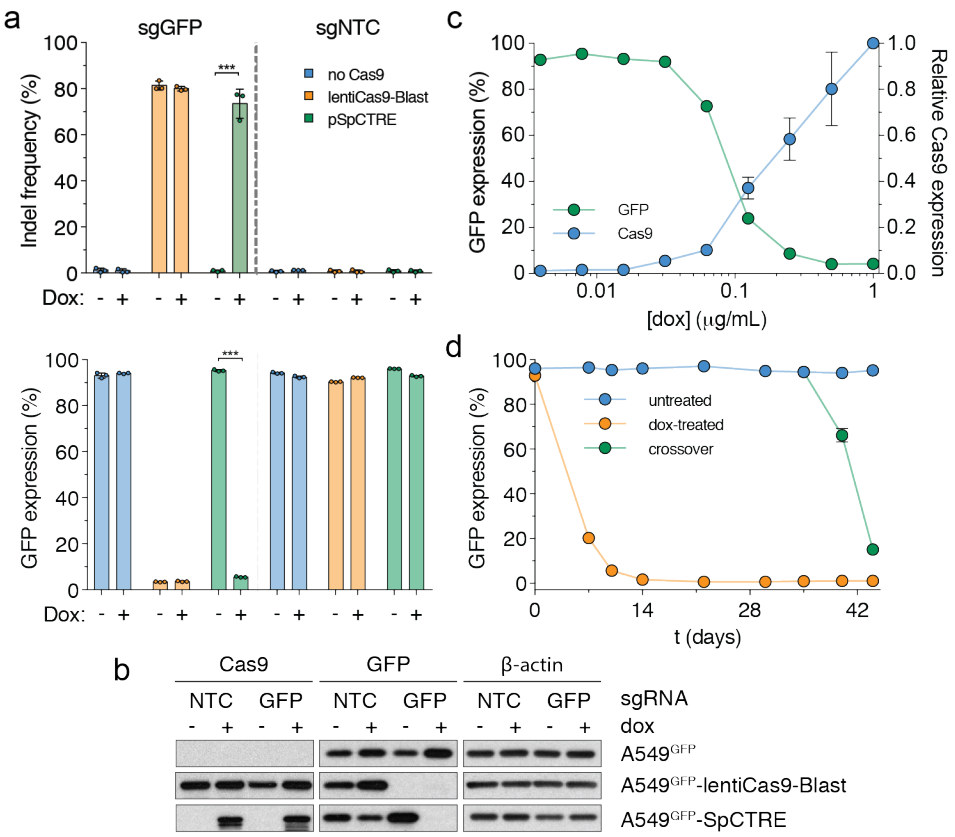

Figure 3.5. pSpCTRE is tightly regulated by dox to facilitate inducible genome editing

(a) *In vitro* genome editing of A549^{GFP} cells lacking Cas9 (blue), with constitutive Cas9 expression from lentiCas9-Blast (orange), or with inducible Cas9 expression from SpCTRE (green) and the indicated sgRNAs. Cells were analyzed for indel frequency (top) and GFP expression (bottom). Error bars are SD (n = 3), SD < plotting character not drawn. *** $p < 0.001$ between groups by two-way ANOVA. NTC, Nontargeting control.

(b) Representative Western blot from GFP editing experiment in (a).

(c) Dox dose response of Cas9 expression and GFP editing in A549^{GFP}-SpCTRE cells with sgGFP. Error bars are SD (n = 3), SD < plotting character not drawn.

(d) Long-term culture of A549^{GFP}-SpCTRE cells with sgGFP untreated (blue) or dox-treated (orange). At day 35, previously untreated cells were crossed over to dox media (green). Error bars are SD (n = 3), SD < plotting character not drawn.

Induced surface expression of $CD4^T$ is a reporter for Cas9 expression and genome editing

An inherent limitation to dox-inducible systems is a lack of uninform transgene induction in a cell population. Dox-inducible lentiviral systems are influenced by local regulatory elements of the genomic locus where they randomly integrate, which can lead to heterogeneous and often poor transgene induction (Loew et al., 2010). This problem can be accentuated *in vivo* by lower tumor dox exposure, relative to *in vitro* culture (Cawthorne et al., 2007). pSpCTRE overcomes this limitation by providing a novel cell surface reporter of dox-induced transgene expression (Fig. 3.6a). This is accomplished by the reverse orientation of the TRE^{3GS} promoter that places it in close proximity to the constitutive EFS promoter that drives $CD4^T$. This promoter topology is unidirectional (low EFS activity only) in the absence of dox and is strongly bidirectional (both EFS and TRE^{3GS} strongly induced) in the presence of dox, thereby increasing $CD4^T$ and Cas9 expression concomitantly (Fig. 3.6a).

This property of pSpCTRE was discovered when we observed an approximately 100-fold increase in $CD4^T$ surface expression from dox treated cells (Fig. 3.6b). We validated that the change in surface expression was a result of increased $CD4^T$ protein expression and correlated with dox doses that induce Cas9 expression (Fig. 3.6c). Importantly, we observed that $CD4^T$ induced cells are a distinct population the can be easily differentiated from uninduced cells in a mixed population (Fig. 3.6d). Rather than a progressive increase in $CD4^T$ signal intensity at increasing dox concentrations, we see a discrete population of $CD4^T$

induced cells emerge (Fig. 3.6d). We speculate that this marked biphasic shift in $CD4^T$ surface expression may be caused by a feed forward loop created by a concurrent increase in rtTA-V10 expression to potently drive bidirectional promoter induction. Therefore, there are three distinct populations of cells to note when using pSpCTRE (Fig. 3.6d):

1) $CD4^T$ negative (pSpCTRE negative)

2) $CD4^T$ positive (pSpCTRE positive, TRE^{3GS} uninduced)

3) $CD4^T$ induced (pSpCTRE positive, TRE^{3GS} induced)

Importantly, $CD4^T$ induced expression is a robust marker of cells that express Cas9 and are competent to undergo Cas9-mediated genome editing. $A549^{GFP}$-SpCTRE cells expressing sgGFP efficiently deplete GFP when treated with 0.25 μg/mL dox and all cells within this population induce $CD4^T$ (Fig. 3.6e). However, at a dox concentration of 0.0625 μg/mL, only ~60% of cells induce $CD4^T$. When we gate these cells based on $CD4^T$ surface expression, GFP is specifically depleted in the $CD4^T$ induced population but not in cells that do not induce $CD4^T$ above baseline. Therefore, we can use $CD4^T$ induction as a marker to enrich for cells that express Cas9 and exclude cells from analysis that do not undergo genome editing. This feature of pSpCTRE allows for identification of cells with efficient and heritable induction of Cas9, enabling the study of heterogeneous tumor cell populations and eliminating the need for selection of single cell clones.

Differential $CD4^T$ surface expression can additionally be exploited by commercial magnetic bead sorting reagents to isolate $CD4^T$ induced cells from a

mixed population (Fig. 3.7). Cells with low levels of constitutively expressed $CD4^T$ are not efficiently bound by dilute α-CD4 magnetic beads and, therefore, are not retained when passed through a magnetic column. Conversely, cells with induced $CD4^T$ are efficiently bound by these same beads and are retained on the magnetic column, providing a mechanism to separate cells based on differential $CD4^T$ surface expression. In essence, this separation protocol allows for the isolation of cells that undergo CRISPR-Cas9 mediated genome editing with a high-throughput and cost-effective approach.

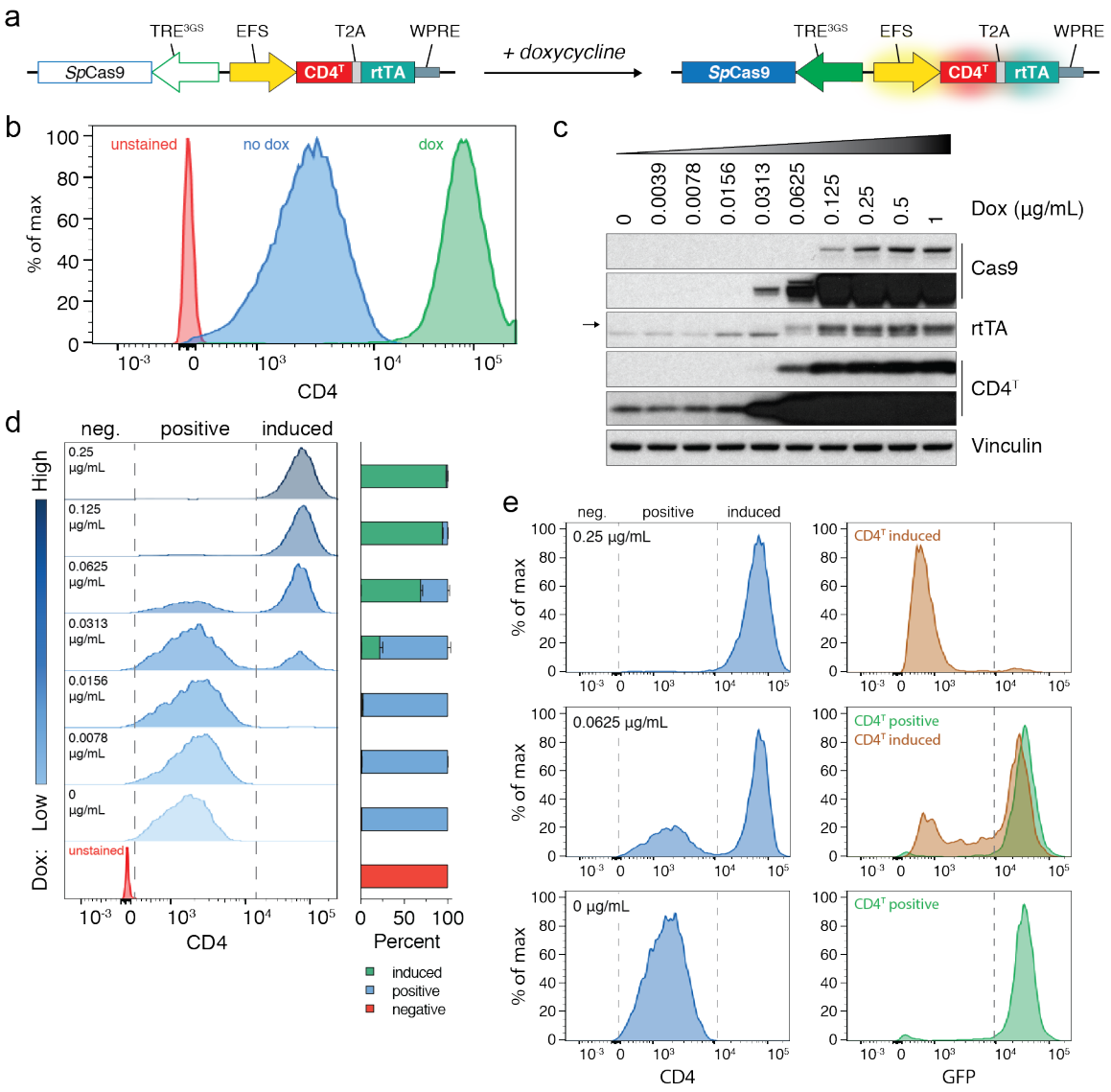

Figure 3.6. Dox induction of EFS promoter activity and CD4^T expression above basal levels is a marker for Cas9 expression and genome editing

(a) Promoter activity and gene expression in the absence (left) or presence (right) of dox is depicted as none (outline), active (solid), and induced (glow). With dox, the TRE^{3GS} promoter is activated while secondarily inducing EFS promoter activity.

(b) Flow cytometry analysis of CD4^T expression in A549-SpCTRE cells treated with (green) or without (blue) dox.

(c) Western blot analysis of A549-SpCTRE cells induced with a range of dox concentrations. Arrow indicates specific rtTA band.

(d) Representative flow cytometry analysis of CD4^T expression with the indicated dox concentrations in A549-SpCTRE cells. Percentage of cells in the negative, positive, and induced gates is displayed in the bar graph (right). Error bars are SD (n = 3), SD < plotting character not drawn.

(e) GFP editing of A549^{GFP}-SpCTRE cells with sgGFP based on gating of CD4^{T} positive or induced populations at the indicated dox doses. Loss of GFP expression is only detected in cells that induce CD4^{T}. Data is representative of three independent experiments.

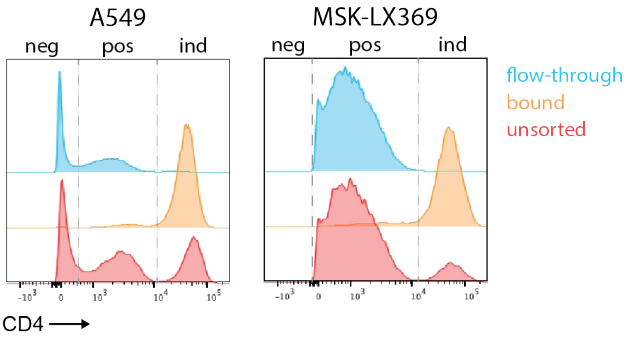

Figure 3.7. Magnetic bead sorting strategy to isolate CD4^T induced cells
Mixed populations of A549 (left) or MSK-LX369 (right) with the indicated CD4^T surface expression were subjected to magnetic bead selection to isolate CD4^T induced cells. Unsorted (red), column bound (orange), and flow-through (blue) cells are as indicated.

sgTrack reporter vectors for tracking clonal dynamics of sgRNA populations

We aimed to develop an sgRNA expression vector that could be used with SpCTRE PDXs to interrogate *in vivo* genetic dependencies. We reasoned that coupling sgRNA expression to a reporter construct would bypass the need for *ex vivo* selection of sgRNA-transduced cells, such as required by pSpCTRE. Instead, the reporter could be used to track the clonal dynamics of sgRNA populations to evaluate fitness effects of gene disruption in a mixed tumor population containing both mouse stromal cells and CRISPR-Cas9 negative tumor cells. To this end, we created sgTrack, which contains a U6 promoter driving sgRNA expression and a Gateway cassette downstream of an EFS promoter (Fig. 3.8a). The Gateway cassette facilitates rapid cloning of a diverse set of reporter constructs to quickly and easily adapt this vector to many downstream applications. One such application is using GFP and mCherry fluorescent reporters to analyze sgRNA populations by flow cytometry (Fig. 3.8b).

We use sgTrack to interrogate genetic dependencies of SpCTRE PDXs or cell lines with a clonal competition assay (Fig. 3.8c). A negative control sgRNA and a test sgRNA targeting a gene of interest are cloned into sgTrack vectors with compatible reporter constructs, such as GFP and mCherry. Cells are independently transduced, admixed at an equal ratio, and either maintained in culture (if cell lines) or engrafted subcutaneously (if PDXs). The fluorescent reporters associated with each sgRNA allow us to measure the relative abundance of sgRNAs in a population as a proxy for the relative fitness of cells engineered to disrupt a gene of interest.

To validate this approach, we performed *in vitro* competition assays targeting the essential gene *RPA1* or the *KRAS* proto-oncogene in A549, a $KRAS^{G12S}$-mutant lung adenocarcinoma cell line. We observed that the GFP:mCherry ratio is stable over 16 days in culture in cells that do not express Cas9, but constitutively expressed Cas9 robustly depletes cells harboring a *RPA1* sgRNA (Fig. 3.9a). Further, depletion of the *RPA1* sgRNA is only observed in A549-SpCTRE cells cultured with dox (Fig. 3.9a). Analysis of competition assays is first done by calculating a fitness score, which is the ratio of cells carrying the test sgRNA to the total number of cells with any sgRNA (Fig. 3.9b). A log ratio is then calculated to measure changes to the fitness score over time or differences in the fitness score between control and dox-treated groups (Fig. 3.9b). Extending this approach, we identified a loss of fitness for cells carrying a *KRAS* sgRNA or a second *RPA1* sgRNA, reflected by the negative log ratio of dox-treated A549-SpCTRE cells (Fig. 3.9c). These experiments highlight the utility of sgTrack reporter vectors for performing clonal competition assays that are well suited to interrogate genetic dependencies *in vivo*.

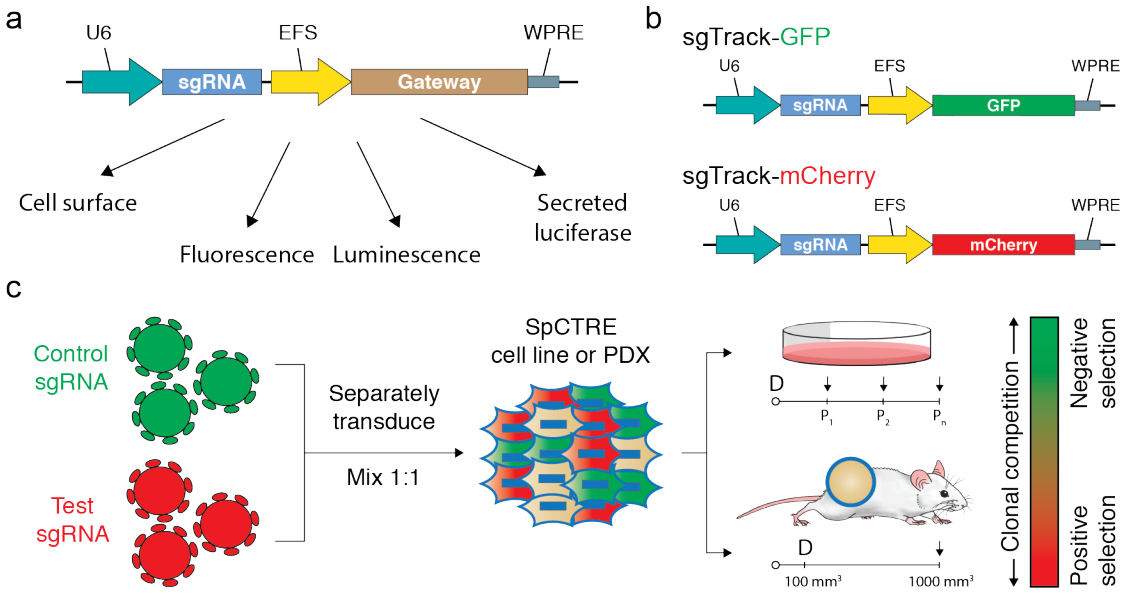

Figure 3.8. sgTrack vectors are a flexible system for tracking clonal dynamics of sgRNA populations

(a) Schematic of sgTrack reporter vector. Reporter constructs are cloned into the Gateway cassette to quickly and easily adapt this vector to many downstream applications.

(b) Schematic of sgTrack-GFP and sgTrack-mCherry vectors.

(c) Schematic of competition assay design. Control or test sgRNAs in sgTrack fluorescent reporter lentiviral vectors are transduced independently into SpCTRE PDXs or cell lines and then admixed and either maintained in culture (if cell lines) or engrafted subcutaneously (if PDXs). Dox addition (D) and flow cytometry analysis (arrows) occurs at the indicated time points and the relative abundance of GFP and mCherry single positive cells is compared between control and dox-treated samples.

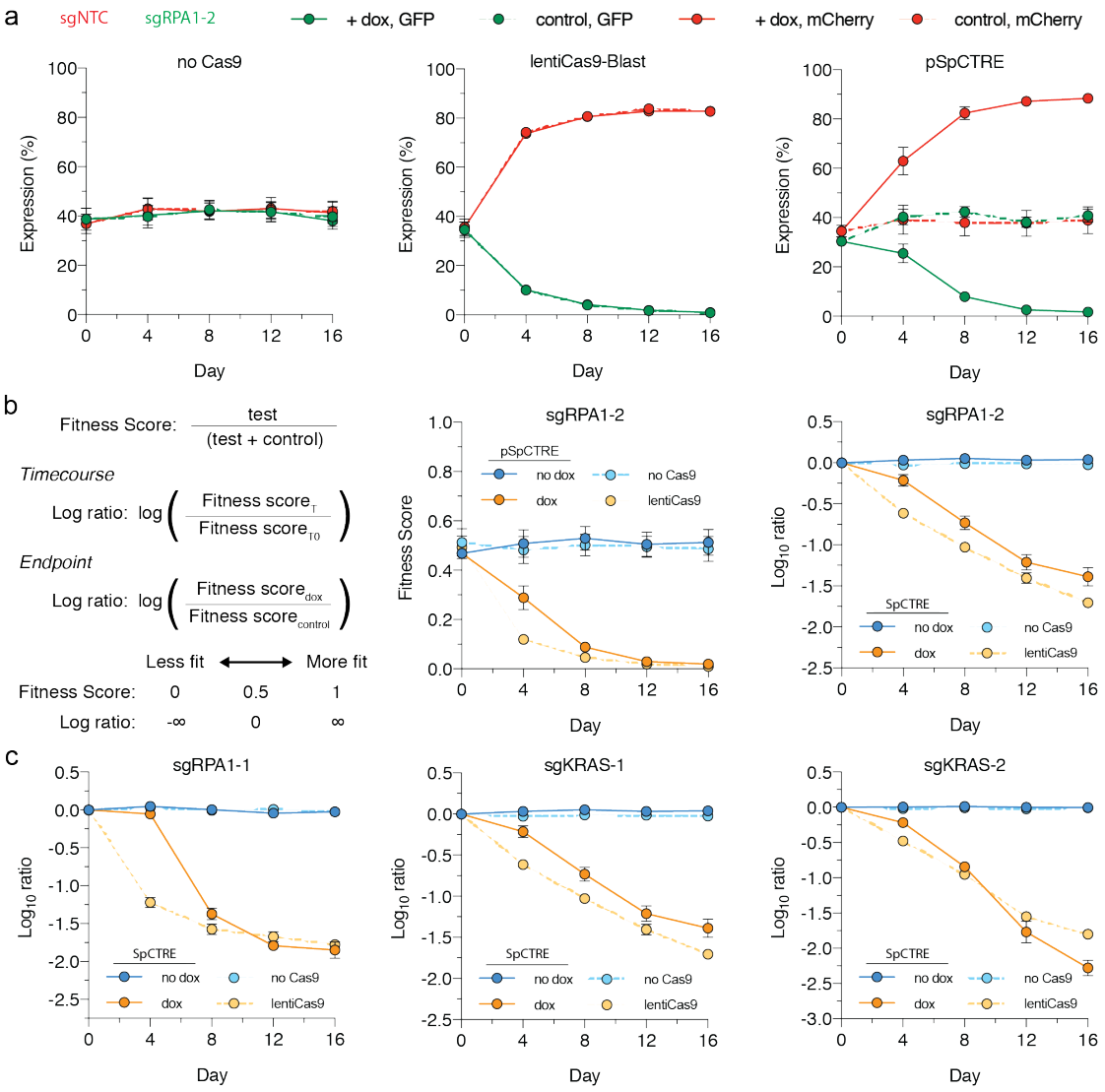

Figure 3.9. Competition assay utilizing sgTrack vectors effectively determines fitness effects of gene disruption

(a) Competition assay of sgRPA1-2 in A549 with no Cas9, constitutive Cas9 expression from lentiCas9-Blast, or dox-inducible Cas9 expression from pSpCTRE (left, middle and right panels, respectively). Competition assays were performed with (solid) or without (dashed) dox. Error bars are SD (n = 3), SD < plotting character not drawn.

(b) Statistical analysis of the competition assay experiment in (a). Fitness score calculates the percent of single positive fluorescent cells with the test sgRNA relative to the total number of single positive fluorescent cells representing both the test and control sgRNAs (coupled here with GFP or mCherry expression, respectively). The log ratio for a timecourse experiment then compares the fitness score at each timepoint to the initial fitness score at T0 or, for endpoint analysis, it compares the fitness score between control and dox-treated groups. A negative log ratio indicates the test sgRNA reduced the fitness of the cells

relative to the control sgRNA. Solid lines represent competition assays in A549-SpCTRE cells either with (orange) or without (blue) dox. Dashed lines represent competition assays in A549 with (orange) or without (blue) Cas9 expression. Error bars are SD (n = 3), SD < plotting character not drawn.
(c) *In vitro* competition assays in A549 with sgRPA1-1, sgKRAS-1, and sgKRAS-2 (left, middle and right panels, respectively). Log ratio calculations and line assignments are as described in (b). Error bars are SD (n = 3), SD < plotting character not drawn.

rAAV for simultaneous delivery of sgRNA and HDR repair template

Precise genome editing by HDR requires a DNA repair template and is stimulated by introduction of a double strand break at the desired genomic locus (Komor et al., 2017). We generated a recombinant adeno-associated virus (rAAV) vector for performing HDR with pSpCTRE that delivers an sgRNA as well as a DNA repair template encoding desired genomic alterations (Fig. 3.10a). The U6-sgRNA-repair template sequence is flanked by multiple cloning sites (MCSs) to facilitate rapid cloning of sgRNAs and their matched DNA repair template. Additionally, a constitutively expressed GFP marker provides a reporter for rAAV transduction.

Point mutations in EGFR are a clinically validated resistance mechanism to EGFR inhibitors (Chong and Jänne, 2013; Thress et al., 2015) and serve as an excellent proof-of-principle for HDR platforms. To edit EGFR, we created an rAAV vector that encodes an sgRNA targeting a sequence proximal to the hydrophobic binding pocket of the EGFR kinase domain and a 1.5-kb repair template centered on this region (Fig. 3.10b). The repair template encodes nucleotide changes that silently destroy the sgEGFR PAM sequence to prevent Cas9 re-cutting after repair and introduces *in cis* 1) a T790M 1st generation EGFR inhibitor gatekeeper mutation, 2) a C797S mutation that abolishes activity of 3rd generation covalent EGFR inhibitors and 3) a silent landmark mutation to experimentally validate that nucleotide changes observed in resistant cells in fact originate from the repair template (Fig. 3.10b).

Efficient generation of osimertinib resistance using this rAAV was evaluated *in vitro* in EGFR-mutant PC9 cells. Cells transduced with rAAV and treated with osimertinib became resistant to treatment after 5 weeks in culture, while osimertinib-treated cells that were not transduced with rAAV remained sensitive to treatment over this same time period (Fig. 3.10c). Sequencing analysis of cells from the rAAV, osimertinib group at day 35 revealed that approximately 80% of EGFR alleles contained the templated C797S mutation (Fig. 3.10d). All of the templated nucleotide changes encoded by the rAAV vector were introduced with the same allele frequency as C797S, confirming template-mediated homology-directed repair. Interestingly, these mutant reads could be detected after only 7 days in culture, even though the bulk population remained sensitive to treatment at this time point (Fig. 3.10d). The IC50 for osimertinib increases from 18.4 nM to 1.15 μM in cells that introduce the templated C797S mutation (Fig. 3.10e). These experiments use a clinically validated resistance mutation to demonstrate efficient genome editing by HDR using our rAAV.

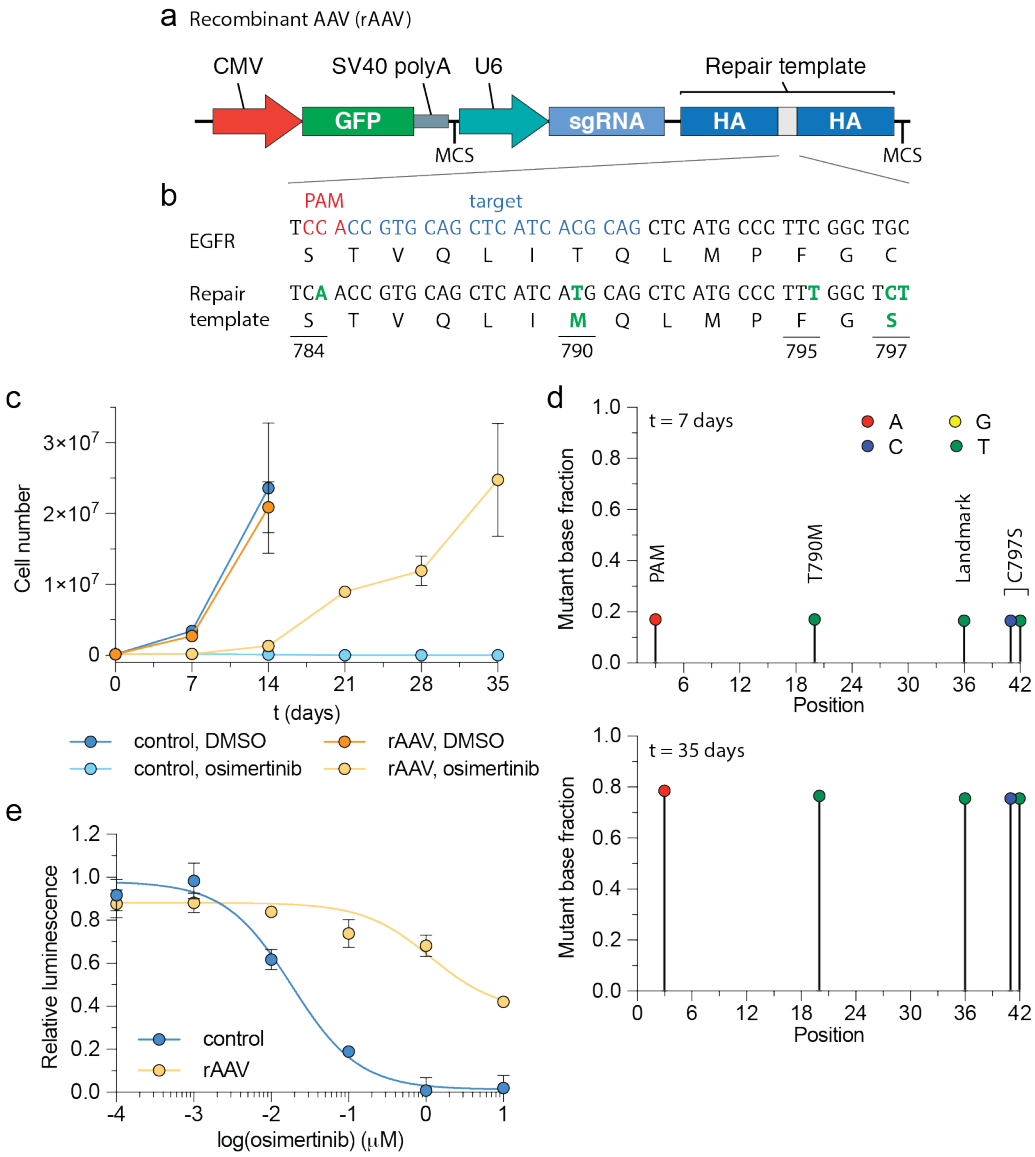

Figure 3.10. rAAV simultaneously delivers sgRNA and homology-directed repair template to drive acquired osimertinib resistance

(a) Schematic of rAAV vector that delivers a GFP marker, an sgRNA expressed from a U6 promoter, and a homology-directed repair template that encodes mutations of interest surrounded by homology arms (HA). The U6-sgRNA and repair template are flanked by multiple cloning sites (MCS)

(b) sgRNA target site and EGFR T790M/C797S repair template to introduce the indicated nucleotide changes (green).

(c) Cell line growth curves of PC9 cells under the indicated conditions. Error bars are SD (n = 3), SD < plotting character not drawn.

(d) Sequencing analysis of PC9 cells from the rAAV, osimertinib group at t = 7 and 35 days.

(e) Osimertinib dose response curves of PC9 cells from the rAAV, osimertinib or control, DMSO treatment arms from panel **a**. Error bars are SD (n = 3), SD < plotting character not drawn.

Discussion

This chapter described the creation of a series of CRISPR-Cas9 vectors designed for *in vivo* functional genomic experiments in PDXs. This platform hinges on pSpCTRE, a dox-inducible Cas9 lentiviral vector that constitutively expresses $CD4^{T}$, a size efficient cell surface marker enabling rapid antibody-based selection of transduced cells. We demonstrated that this vector is tightly regulated by dox and is able to drive sufficient expression of Cas9 for genome editing applications. We further created sgTrack to enable clonal tracking of sgRNA populations and a rAAV vector to deliver a DNA repair template along with an sgRNA for precise genome editing via HDR. These vectors constitute the first CRISPR-Cas9 vectors designed specifically for use in PDXs and, through *in vitro* experiments, we demonstrate that they possess the necessary properties for *in vivo* genome editing applications.

Multiple aspects of these CRISPR-Cas9 vectors we designed to enable flexibility in the design and execution of *in vivo* functional genomic experiments. A Gateway cassette within sgTrack allows reporter constructs to be quickly interchanged depending on the downstream application. In this thesis, we use fluorescent reporter vectors to analyze the clonal dynamics of sgRNA populations in PDXs and in culture. However, a luciferase reporter could be used to analyze how gene disruption affects metastasis in PDXs grown orthotopically (Hoffman, 2015), while secreted luciferase reporters would enable clonal sgRNA dynamics to be analyzed over time through routine blood collection, rather than only at the endpoint of an experiment (Charles et al., 2014;

van Rijn et al., 2013). Additionally, the MCS within rAAV provides sites to quickly clone in paired sgRNA-DNA repair template gene synthesis fragments and could easily be multiplexed to study multiple repair templates in a single pooled experiment (Findlay et al., 2014; Winters et al., 2017).

The bidirectional promoter induction that serves to induce $CD4^T$ expression concomitantly with Cas9 expression is an important feature of pSpCTRE. We show that induced $CD4^T$ expression can not only be used to identify cells that undergo Cas9-mediated genome editing, but can also be exploited by magnetic bead separation to specifically isolate cells with induced $CD4^T$ (Fig. 3.7). This could be exploited to purify cells from a mixed population with specific genes disrupted to perform indel analysis or RNA-sequencing on this population.

CHAPTER 4

Utilizing SpCTRE PDXs to perform *in vivo* functional genomics

Introduction

Patient-derived xenografts (PDXs) constitute a powerful set of preclinical models for *in vivo* cancer research, reflecting the spectrum of genomic alterations and therapeutic liabilities of human cancers (Bruna et al., 2016; Drapkin et al., 2018; Krepler et al., 2017; Townsend et al., 2016). These models recapitulate the complex genotypes and intratumoral heterogeneity of their tumors of origin and are not subject to the selective pressures imposed by *in vitro* cell culture since they are maintained exclusively *in vivo* (Daniel et al., 2009; Guo et al., 2016; Poirier et al., 2015). In addition, PDXs have proven to be valuable models of tumor types or genetic alterations for which *in vitro* models are not readily available (Beshiri et al., 2018; Puca et al., 2018). These features have driven the rapid adoption and widespread use of PDXs in preclinical and co-clinical oncology drug development, evaluation of biomarkers and imaging agents, and mechanistic investigation of acquired treatment resistance (Gao et al., 2015; Gardner et al., 2017; Lallo et al., 2017).

In the previous chapter, we developed a platform for CRISPR-Cas9 genome editing tailored for use in PDXs. We validated the utility of this platform with *in vitro* models and found it to contain the requisite properties for use in PDXs, namely tight regulation by dox, efficient editing in the induced state, and a

cell surface marker suitable for rapid non-pharmacologic *ex vivo* selection. Additionally, the bidirectional promoter topology utilized in pSpCTRE creates a cell surface marker for Cas9 induction and should further increase the utility of this system for *in vivo* genome editing. The accompanying sgRNA vectors for reporter based clonal competition assays and precise genome editing via HDR set up this platform to perform a wide range of functional genomic experiments in PDXs.

In this chapter, we investigate the ability of this CRISPR-Cas9 platform to be used for *in vivo* genome editing experiments in PDXs. We generate a library of lung cancer SpCTRE PDXs that are capable of inducibly expressing Cas9 and use these models to interrogate *in vivo* genetic dependencies. Finally, using an EGFR mutant SpCTRE PDX, we introduce clinically validated EGFR inhibitor resistance mutations to demonstrate the ability of this platform to generate precise sequence alterations by homology-directed repair. This genome editing platform significantly enhances the utility of PDXs as genetically programmable models of human cancer.

Results

Generating a library of SpCTRE PDXs

Routine passaging of established PDXs provides an opportunity to quickly perform an *ex vivo* lentiviral transduction in these models. Typically, PDXs are dissociated to a single cell suspensions using enzymatic digestion and viable

cells are admixed with matrigel to reimplant into a subsequent generation host mouse, a process that takes approximately 2-3 hours (Mattar et al., 2016). For generating SpCTRE PDXs, we take advantage of this brief period outside the mouse to perform an *ex vivo* spin transduction, which only adds 1 hours to the total processing time. This quick infection step minimizes the amount of time cells are not in an *in vivo* environment.

Cas9-expressing SpCTRE PDXs can be generated in as few as two *in vivo* passages. In the first passage, dissociated tumors are subjected to an *ex vivo* spin transduction and immediately re-engrafted for expansion *in vivo*. Successfully transduced cells are enriched from the ensuing tumor with α-CD4 positive selection and either cryopreserved or passaged for subsequent use in functional genomic studies (Fig. 3.1.b).

We sought to generate a library of SpCTRE PDXs and transduced 20 PDXs representing multiple lung cancer subtypes with pSpCTRE lentivirus. We were able to detect and enrich $CD4^T$ positive cells in six of these models (Fig. 4.1a). In the 14 remaining models, no $CD4^T$ positive cells were detected following pSpCTRE transduction. The median time to establish SpCTRE PDXs following transduction was 154 days (with a range of 108 to 305 days) and one to three *in vivo* passages were required after transduction (Fig. 4.1b). Importantly, these SpCTRE PDX tumors express Cas9 exclusively when the mice are administered dox (Fig. 4.1c).

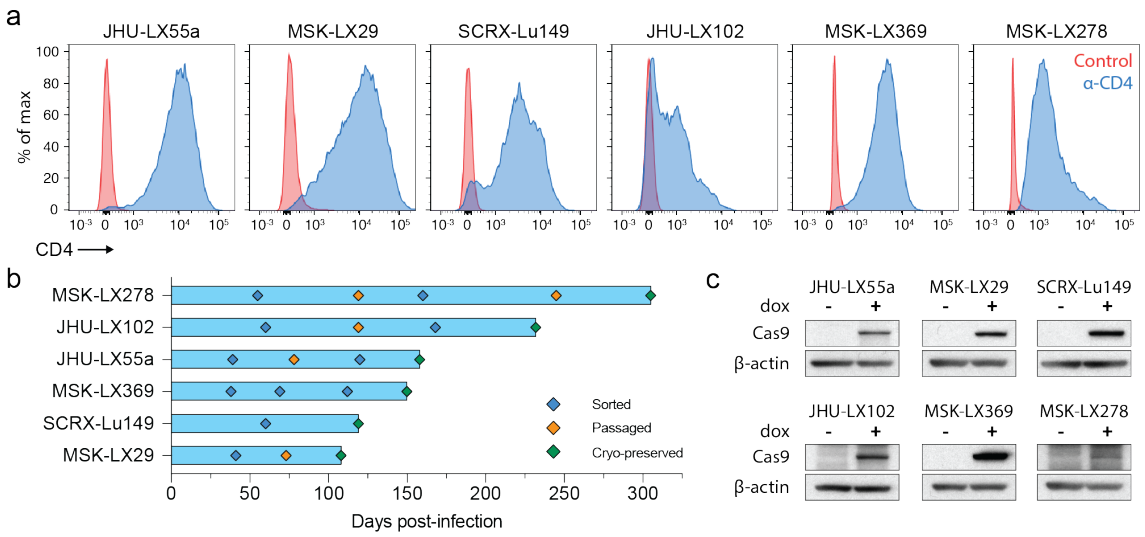

Figure 4.1. Generation of Cas9-expressing PDXs using pSpCTRE
(a) $CD4^T$ staining of SpCTRE PDXs successfully transduced with pSpCTRE lentivirus and enriched for $CD4^T$ positive cells using FACS. Control is fluorescence minus one (FMO) that excludes α-CD4 antibody.
(b) Timeline for SpCTRE PDX model generation. PDXs were 1) sorted to enrich for $CD4^T$ positive cells if $CD4^T$ positive percentage was below 50% (blue), 2) passaged to expand for additional sorting or cryopreservation (orange), or 3) cryopreserved (green).
(c) Western blot analysis of Cas9 expression in the indicated pSpCTRE PDXs from control or dox-treated mice.

Interrogating genetic dependencies in SpCTRE PDXs

Interrogating genetic dependencies in SpCTRE PDXs is potentially confounded by 1) mouse stromal cell content and 2) SpCTRE-positive tumor cells that do not induce Cas9 expression. Mouse stromal cell content varies significantly between PDXs and, in some cases, can exceed 50% of the total cells within a PDX tumor (Schneeberger et al., 2016). Further, dox-induced transgene expression in xenograft tumors is highly dynamic and can differ greatly depending on the delivery method used (Cawthorne et al., 2007). For SpCTRE PDXs, this can lead to heterogeneous Cas9 induction and gene disruption. These factors highlight the need for an internally controlled clonal competition assay that does not rely on bulk tumor volume measurements to assess fitness effects of gene disruption (Fig. 3.8c). The fluorescent reporter sgTrack vectors permit analysis of clonal competition assays by flow cytometry, where mouse stromal cells can be excluded from analysis and tumor cells can be gated based on $CD4^T$ surface expression to identify SpCTRE PDX cells that induce Cas9.

Induced $CD4^T$ surface expression is a robust marker for genome editing *in vitro* (Fig. 3.6e) and we first sought to explore the utility of this marker for SpCTRE PDXs *in vivo*. We performed a clonal competition assay in MSK-LX369-SpCTRE with sgTrack-mCherry/sgRPA1-1 and sgTrack-GFP/sgNTC and observed a discrete population of $CD4^T$ induced cells in tumors from dox-treated mice (Fig. 4.2a). $CD4^T$ positive cells from control or dox-treated mice contained similar percentages of the two sgRNAs, with sgTrack-mCherry/sgRPA1-1 cells making up greater than 65% of the population and no difference in the log ratio

between these two groups (Fig. 4.2b, c). However, cells from dox-treated mice with induced $CD4^T$ surface expression had a strong depletion in cells harboring sgRPA1-1. This population consisted of fewer than 15% $mCherry^+$ cells and there was a significant decrease in the log ratio of $CD4^T$ induced cells from dox-treated mice relative to control mice (Fig. 4.2b, c). To further confirm the utility of $CD4^T$ induction as a marker for genome editing *in vivo*, we sorted $mCherry^+$ cells from these $CD4^T$ populations to analyze indel formation at the *RPA1* locus. We observed *RPA1* editing specifically in $CD4^T$ induced cells from dox-treated mice and, importantly, no editing was detected in $CD4^T$ positive cells from control or dox-treated mice (Fig. 4.2d). These data verify $CD4^T$ induction as an *in vivo* marker for Cas9 expression and genome editing.

We next performed *in vivo* competition assays to study the effects of single gene disruption on the fitness of three SpCTRE PDXs. Targeting *RPA1* in MSK-LX369, JHU-LX55a, and MSK-LX29, we consistently observed a significant depletion of cells carrying the *RPA1* sgRNA (Fig. 4.3a-c). $CD4^T$ induction in these models ranged from 1-20% of tumor cells (Fig. 4.3a-c). Additionally, we investigated the fitness effects of *KRAS* gene disruption in two KRAS-mutant lung adenocarcinoma SpCTRE PDXs, MSK-LX369 and JHU-LX55a. We observed a significant depletion of cells harboring KRAS sgRNAs in $CD4^T$ induced cells from dox-treated mice, indicating that these PDXs exhibit reduced fitness in the context of *KRAS* disruption (Fig. 4.3a, b). These experiments verify that this system is suited to functionally interrogate PDX gene essentiality *in vivo*.

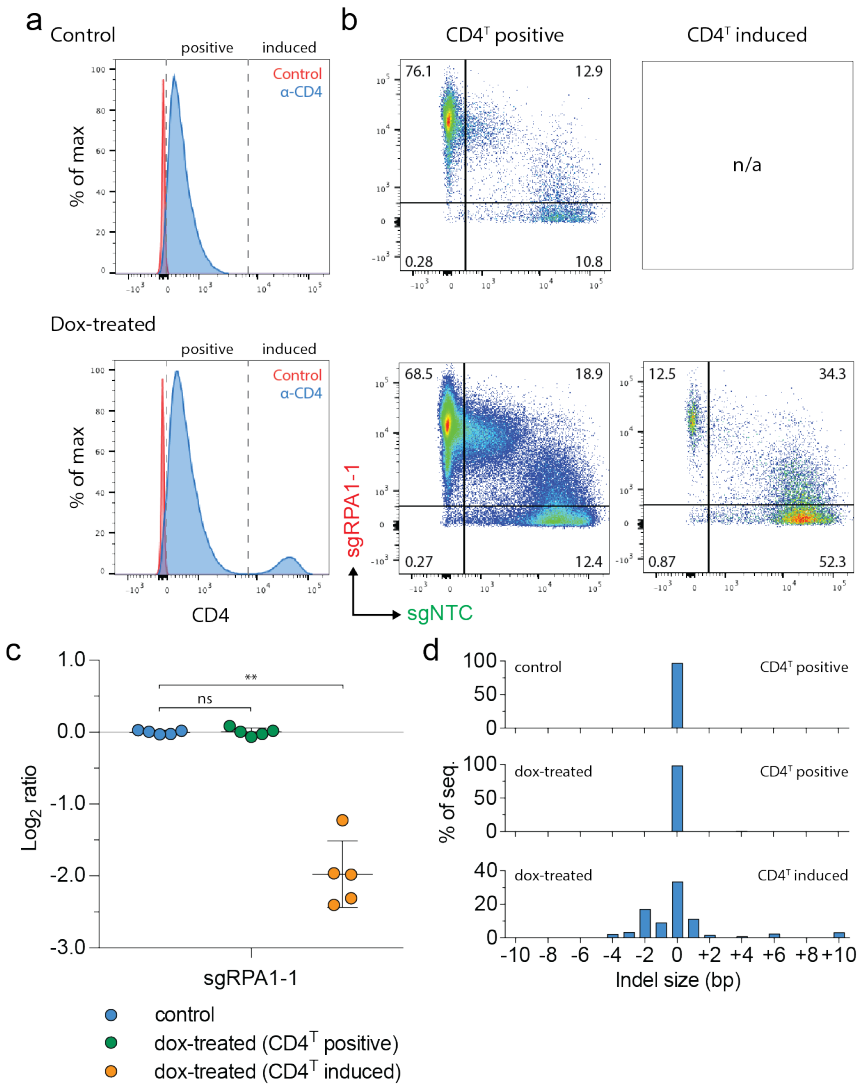

Figure 4.2. Genome editing in SpCTRE PDXs is restricted to CD4^T induced population

(a) Representative histograms of CD4^T surface expression in MSK-LX369-SpCTRE tumors from control (top) or dox-treated mice (bottom) in an sgRPA1-1 competition assay.

(b) Representative flow cytometry dot plots displaying percentage of cells harboring sgRPA1-1 (mCherry) or sgNTC (GFP) in MSK-LX369-SpCTRE tumors from control or dox-treated mice gated based on CD4^T surface expression as shown in panel (a).

(c) Analysis of sgRPA1-1 competition assay in MSK-LX369-SpCTRE tumors. Dox-treated tumors were gated on CD4^T surface expression before analysis as shown in panel (a). Log ratio was calculated as described in Figure 3.9b. Error bars are SD (n = 5), SD < plotting character not drawn. Each data point represents one tumor. * $p < 0.05$ and ** $p < 0.01$ between groups by Wilcoxon rank sum test.

(d) Representative indel analysis of mCherry^{+} cells harboring sgRPA1-1 in MSK-LX369-SpCTRE tumors from control or dox-treated mice sorted based on CD4^{T} surface expression as shown in panel (a).

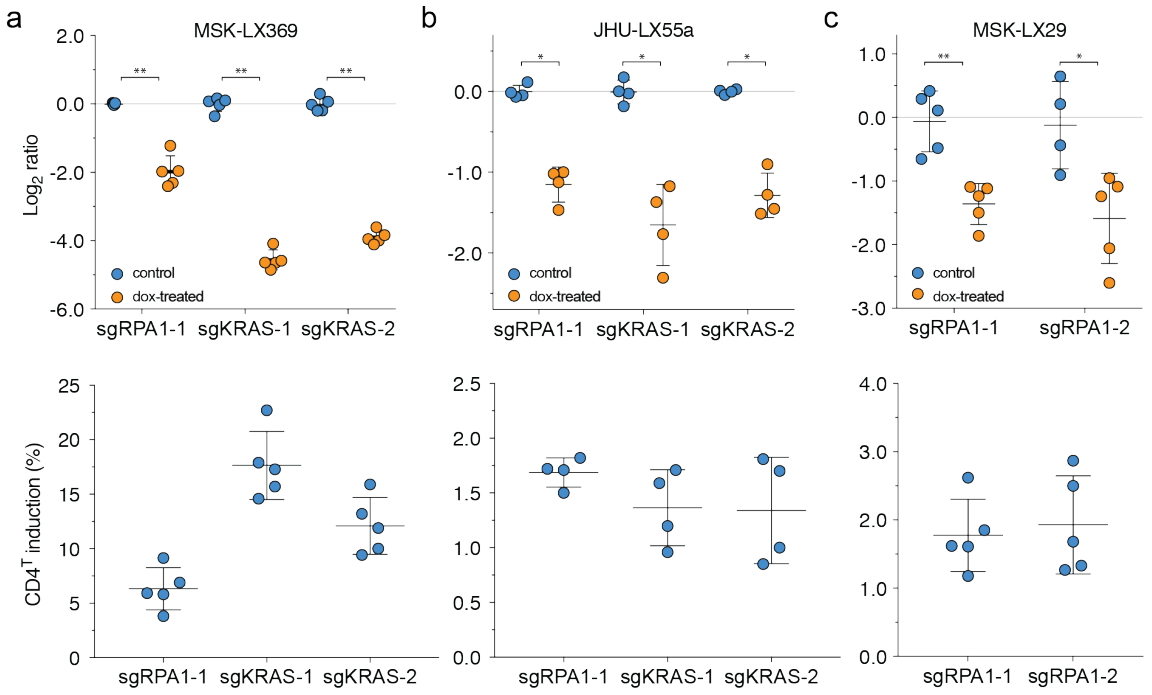

Figure 4.3. Interrogation of genetic dependencies in SpCTRE PDXs using a competition assay

(a-c) Competition assays analysis (top) and percent of cells with induced $CD4^T$ surface expression from dox-treated mice (bottom) with the indicated sgRNAs in the SpCTRE PDXs (a) MSK-LX369, (b) JHU-LX55a, and (c) MSK-LX29. Dox-treated tumor analysis was restricted to cells with induced $CD4^T$ surface expression. Log ratio was calculated as described in Figure 3.9b. Error bars are SD (n = 4-5), SD < plotting character not drawn. Each data point represents one tumor. * $p < 0.05$ and ** $p < 0.01$ between groups by Wilcoxon rank sum test.

Precise genome editing of SpCTRE PDXs using HDR

To interrogate the use of SpCTRE PDXs for CRISPR-Cas9 mediated HDR we again used our rAAV construct including base substitutions in EGFR known to drive resistance to EGFR first- and third-generation TKIs in EGFR-mutant lung adenocarcinomas. MSK-LX29 was derived from a patient whose tumor carried a homozygous $EGFR^{L858R}$ mutation and who developed resistance to the 1st generation EGFR inhibitor erlotinib through acquisition of a focal *MET* amplification. This PDX is resistant to single agent treatment with the 3rd generation EGFR inhibitor osimertinib as well as the MET inhibitor crizotinib but is profoundly sensitive to a crizotinib-osimertinib (C/O) combination therapy (Fig. 4.4a). While p-EGFR and p-MET are inhibited by osimertinib and crizotinib single agent treatment, respectively, phosphorylation of both receptors is more potently inhibited by the C/O combination therapy (Fig. 4.4b). Based on these data, we reasoned that restoring EGFR activity by introducing the osimertinib resistance mutation C797S via HDR would be sufficient to induce resistance of MSK-LX29 to C/O combination therapy.

MSK-LX29-SpCTRE cells were infected *ex vivo* with the previously described rAAV construct encoding EGFR TKI resistance alleles including C797S, and subsequently engrafted into dox-treated mice to induce Cas9 expression and initiate HDR (Fig. 4.5a). These tumors were initially sensitive to C/O combination therapy, which may reflect the latency of Cas9 expression in response to dox treatment or the preference for the NHEJ repair pathway in mammalian cells (Lieber, 2010; Mao et al., 2008). However, 2 weeks after the

start of treatment MSK-LX29-SpCTRE developed resistance in all five tumors in the rAAV plus C/O treatment group, but in none of the C/O treated tumors not infected with rAAV (Fig. 4.5b). This observation is consistent with the clonal outgrowth of a subpopulation of cells that successfully introduced the C797S mutation via HDR. Sequencing of all five resistant tumors revealed the presence of the templated C797S mutation, accompanied by all the other single nucleotide changes present in the repair template (Fig. 4.5c, d). We conclude that an acquired resistance mutation in EGFR alone is sufficient to restore resistance to crizotinib-osimertinib combination therapy in EGFR mutant lung adenocarcinomas that acquire bypass resistance through *MET* amplification. More generally, these data confirm that pSpCTRE, in combination with rAAV, can be used to introduce complex template-directed site-specific mutations into PDXs *in vivo*.

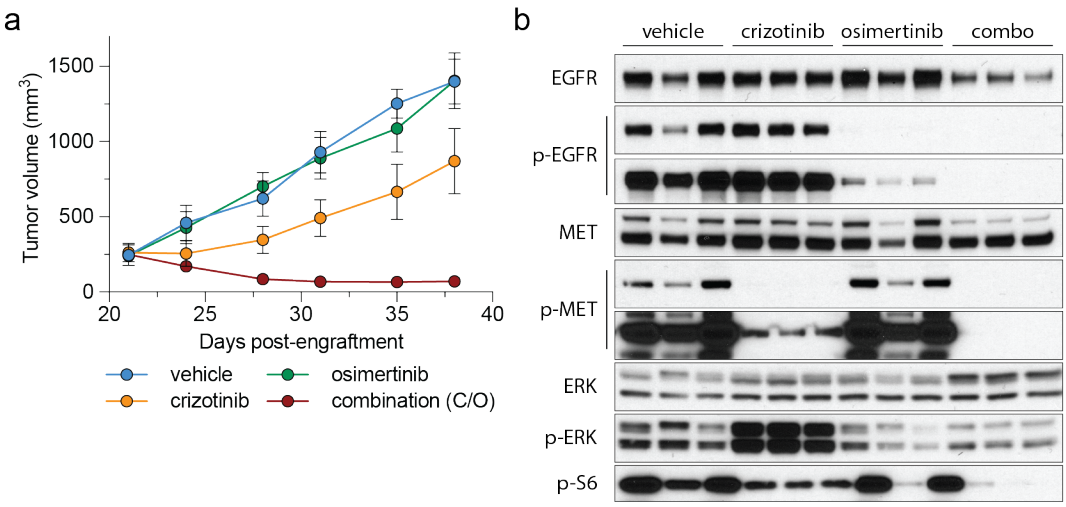

Figure 4.4. Evaluation of EGFR inhibitor combination therapy in *MET* amplified PDX

(a) MSK-LX29 tumor growth curves for the indicated treatment arms. Error bars are SD (n = 3), SD < plotting character not drawn. C/O, crizotinib/osimertinib combination.

(b) Western blot analysis of the tumors treated in (a).

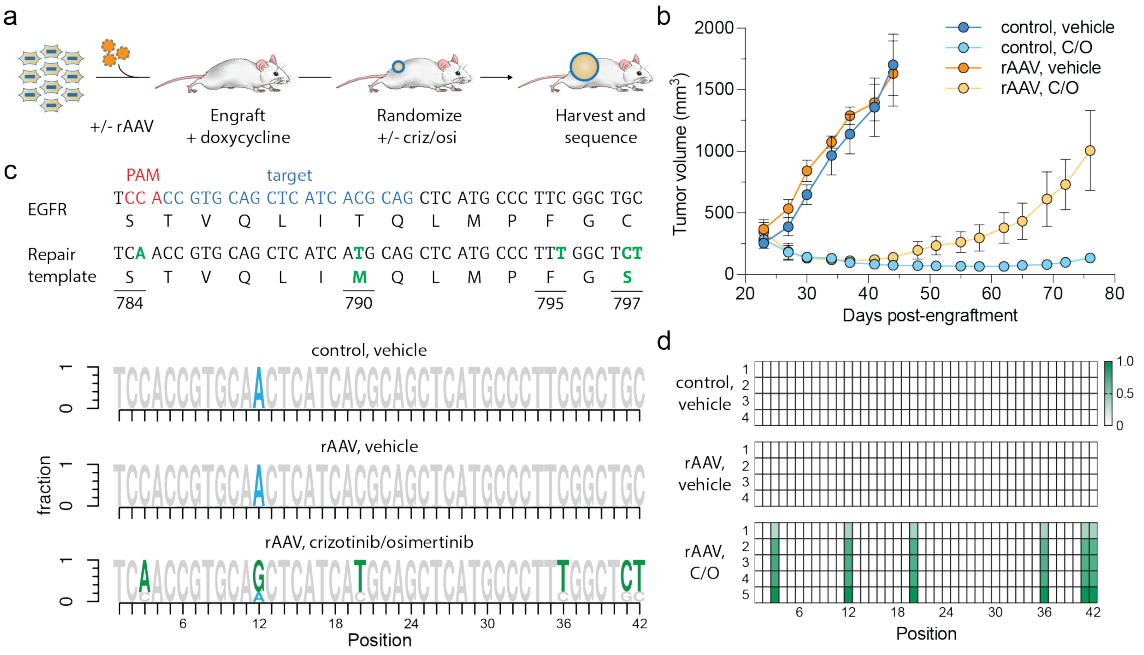

Figure 4.5. Introduction of complex drug resistance mutations in SpCTRE PDXs using rAAV

(a) Schematic of EGFR editing experiment in MSK-LX29-SpCTRE. Dissociated tumor cells were infected with rAAV and immediately engrafted. Mice were administered dox at the time of tumor engraftment and randomized to treatment groups once tumors reached approximately 250 mm^3. Tumors were collected for sequencing once they reached > 1000 mm^3.

(b) Tumor volumes of MSK-LX29-SpCTRE with or without rAAV and treated with a crizotinib/osimertinib (C/O) combination or vehicle. Error bars are SD (n = 5), SD < plotting character not drawn.

(c) Sequencing analysis of representative tumors from the indicated treatment groups. Mutations introduced by rAAV are highlighted (green). MSK-LX29 contains a homozygous SNP (blue) that is removed by the rAAV.

(d) Heatmap depicting frequency of rAAV introduced mutations for tumors from the indicated treatment groups.

Discussion

In this chapter, we generated a library of SpCTRE PDXs and validated the utility of these models for *in vivo* functional genomic experiments. Using sgTrack, we targeted the essential gene *RPA1* and found that we could indeed generate indels specifically in $CD4^T$ induced cells. Further, we verified that our clonal competition assay could be used to interrogate *in vivo* genetic dependencies as we consistently observed a decrease in the fitness of SpCTRE PDX cells with *RPA1* or *KRAS* gene disruption. In MSK-LX29-SpCTRE, an EGFR-mutant lung adenocarcinoma PDX from a patient that became resistant to EGFR TKI through a *MET* amplification, we were able to use a rAAV to introduce EGFR drug resistance mutations via HDR. These data indicate that SpCTRE PDXs can be successfully used for *in vivo* functional genomic applications.

One limitation with the current system is the inability to transduce all PDXs with pSpCTRE lentivirus. We were able to generate 6 SpCTRE PDXs in this study, however we were unsuccessful in generating SpCTRE PDXs for the remaining 14 PDXs attempted. In each case, the failure was due to a lack of lentiviral transduction as no $CD4^T$ positive cells could be detected. Transduction efficiency varies greatly between different cell types (Sastry et al., 2002; Zhang et al., 2004) and it is possible that further increasing the titer of pSpCTRE could improve the success rate of transducing PDXs. However, it is also possible that these failed PDXs are unable to be transduced with VSV-G pseudotyped lentivirus. In these situations, non-viral delivery methods could be explored, such

as knock-in to the *AAVS1* safe harbor locus, to achieve stable integration of the pSpCTRE cassette without lentiviral transduction.

Another limitation with these experiments is the restricted numbers of cells that induce Cas9, as we consistently observe fewer than 5% of SpCTRE PDX cells within a tumor induce $CD4^T$ expression (Fig. 4.3). While we can gate cells based on $CD4^T$ surface expression to analyze clonal competition assays, further applications of SpCTRE PDXs could be limited by this low percentage of induction. For instance, a CRISPR screen would require 20 times as many mice to achieve the same representation of the sgRNA library if only 5% of the SpCTRE PDX cells induce Cas9. In generating MSK-LX369-SpCTRE, we placed the mice on dox chow in the first passage after pSpCTRE transduction and sorted $CD4^T$ induced cells from the resulting tumor. While this approach increased the number of passages required to generate the SpCTRE PDX model (Fig. 4.1), we observed that up to 20% of cells were now able to induce Cas9 in clonal competition experiments (Fig. 4.3a). Sorting for $CD4^T$ induced cells could be added to the protocol for generating SpCTRE PDXs to enrich for cells with heritable Cas9 induction and facilitate additional CRISPR applications.

CHAPTER 5

DISCUSSION

The high failure rate for developing new cancer therapeutics can be attributed in part to the extensive use of preclinical models that do not accurately recapitulate many aspects of human tumors (Tentler et al., 2012). PDXs are high fidelity cancer models that maintain several important features of the tumors from which they were derived, including mutational, gene expression, and epigenetic profiles (Daniel et al., 2009; Guo et al., 2016; Poirier et al., 2015), and therefore are valuable tools for elucidating novel aspects of tumor biology. However, the use of PDXs in cancer research is limited to a narrow scope of applications that exclude most types of mechanistic experiments due to the technological barriers imposed by continuous *in vivo* heterotransplantation. We have developed herein methods for CRISPR-Cas9 genome editing of PDXs while maintaining growth exclusively *in vivo*.

Although these methods were developed with primary xenografts in mind, this system is readily applicable to other model systems. Unlike mouse organoid cultures, which can be derived from mice engineered with conditional Cas9 expression, human primary organoid explants are subject to many of the same experimental challenges as primary tumor xenografts, suggesting that pSpCTRE constructs would prove particularly useful in this setting. The pSpCTRE cassette may also be useful as the basis for improved general-purpose doxycycline

inducible constructs, such as in the context of *Col1A1* targeting vectors, which have shown variable degrees of doxycycline control across different adult mouse tissues (Beard et al., 2006; Dow et al., 2012).

Several aspects of these methods could be improved to enable more complex experimental designs. The current iteration of the clonal competition assay is limited to endpoint analysis of a single genetic perturbation for each *in vivo* experiment. Future work could address these limitations as needed with new constructs encoding diverse reporters. Secreted luciferases have been used as a surrogate for population size in cell line xenografts and would be equally applicable in this setting (Charles et al., 2014; van Rijn et al., 2013). Multiplexing of tens to hundreds of sgRNAs could be made possible by coupling each genetic perturbation to the expression of a unique cell surface protein epitope, significantly increasing the throughput of the system (Stoeckius et al., 2017; Wroblewska et al., 2018). Similar focused screens of targeted pools of sgRNA may be possible using standard sequencing approaches to quantify changes in sgRNA abundance under different experimental conditions (Poirier, 2017). Exploration of highly diversified sequence space of a single genomic locus, as previously demonstrated with rAAV in genetically engineered mouse models, would be equally applicable to SpCTRE-PDX (Winters et al., 2017).

This initial pSpCTRE construct encodes SpCas9; however, future iterations could employ Cas9 variants with increased fidelity, expanded PAM specificity, or altered enzymatic activity to enable a range of other genetic manipulations in PDXs (Casini et al., 2018; Hu et al., 2018; Kleinstiver et al.,

2016; Komor et al., 2016). Still, use of these Cas9 variants would require repeating the lengthy transduction and enrichment steps, which can take more than 6 months to generate SpCTRE PDXs in some cases. One interesting approach would be to use dead sgRNAs (dgRNAs), which are truncated sgRNAs that recruit wild-type Cas9 to specific genomic loci but do not generate DSBs, effectively converting Cas9 to dCas9 (Liao et al., 2017). These dgRNAs can then be combined with an MS2 RNA scaffold to recruit proteins with additional functions and elicit transcriptional activation or epigenetic modification. Importantly, dgRNAs could be used with existing SpCTRE PDXs, thereby circumventing the lengthy process that would be required to create PDXs expressing dCas9.

$CD4^T$ was chosen as the cell surface selection marker in part because PDXs are primarily grown in immunodeficient mice that lack lymphocytes. However, recent methods have been developed to establish PDXs in mice with humanized immune systems for cancer immunotherapy studies (Wang et al., 2018). While $CD4^T$ lacks the cytoplasmic domain required for intracellular signaling, we cannot rule out the possibility that it may confound the results of such studies. Accordingly, pSpCTRE could be adapted with an alternative cell surface selectable marker, such as ΔLNGFR (Bonini et al., 1997) or huEGFRt (Wang et al., 2011b), for these purposes. An additional challenge that may arise in using SpCTRE PDXs with humanized mice is the potential for both Cas9 and sgRNAs to elicit an immune response (Charlesworth et al., 2019; Wienert et al., 2018). This could lead to direct T-cell mediated cytotoxicity or alter the immune

microenvironment of SpCTRE PDXs grown in humanized mice and greatly affect immunotherapy studies.

A natural extension of the work presented in this thesis is to perform pooled CRISPR screens in SpCTRE PDXs to identify *in vivo* genetic dependencies with a high throughput approach. While the design and execution of these screens has become routine for *in vitro* models (Miles et al., 2016), several aspects of SpCTRE PDXs present challenges for adapting this approach to *in vivo* models and must be taken into consideration. First, xenograft tumor engraftment can create a clonal bottleneck whereby a minority of injected tumor cells successfully engraft to form the resulting tumor (Quintana et al., 2008). Clonal bottlenecking must be corrected for when designing a screen as this can lead to decreased representation of the sgRNA library and reduced statistical power to accurately determine candidate genetic dependencies (Bossi et al., 2016). Performing the screen in several parallel tumors could overcome this issue, however, the extent of clonal bottlenecking will vary for each PDX model and must be empirically determined prior to performing a CRISPR screen in that model. A small, focused sgRNA library could facilitate an *in vivo* CRISPR screen by allowing for adequate representation of the library in a practical number of tumors.

Another approach to increasing the statistical power of an *in vivo* CRISPR screen is to employ an sgRNA library with unique molecular identifier (UMI) barcodes (Michlits et al., 2017). With this method, each cell infected with a particular sgRNA contains a unique barcode that can be used to track the clonal

dynamics of sgRNA populations at single-cell resolution. The primary benefit of this approach is in elucidating fitness effects of gene disruption in settings with high clonal variance, as is the case with *in vivo* xenograft tumors. The UMI barcode minimizes the effects of clonal bottlenecking since it can be used to determine the number of cells with each sgRNA that successfully engraft and under represented sgRNAs can be subsequently excluded from analysis. Further, this approach can more robustly identify moderate growth phenotypes that may be of interest for further validation experiments.

Finally, a CRISPR screen in SpCTRE PDXs is complicated by the variable amount of Cas9 induction observed after mice are administered dox (Fig. 4.3a-c). This creates a problem for analyzing *in vivo* loss of function screens that infer fitness effects of gene disruption by sequencing the bulk tumor population to determine relative sgRNA abundance. sgRNAs will be present in cells that do not induce Cas9 and therefore create a high background signal that will make it difficult to identify depleted sgRNAs and candidate genetic dependencies. Improving the inducibility of Cas9 in SpCTRE PDXs could reduce this background signal and facilitate loss of function CRISPR screens in these models. One method for achieving this is by administering dox during the model generation process and sorting $CD4^{T}$ induced cells, thereby enriching cells that are heritably capable of inducing Cas9. This approach was used in generating MSK-LX369, which exhibits Cas9 induction in a greater proportion of cells than either MSK-LX29 or JHU-LX55a (Fig. 4.3a-c). However, Cas9 induction is still

limited to a maximum of 20% of the tumor cells in MSK-LX369 and would still pose a significant challenge in analyzing a CRISPR screen in this model.

An alternative approach to analyzing a CRISPR screen in SpCTRE PDXs would be to restrict sequencing only to $CD4^T$ induced cells rather than the bulk tumor population. We showed that $CD4^T$ induced cells were able to be separated from $CD4^T$ negative and $CD4^T$ positive cells using magnetic bead sorting for both SpCTRE cell lines and PDXs (Fig. 3.7). Magnetic bead sorting is more cost effective with higher throughput than FACS and a potential screen workflow could incorporate this sorting to separate $CD4^T$ positive and $CD4^T$ induced cells prior to sequencing analysis. Additionally, sequencing of the $CD4^T$ positive cells would minimize noise created by clonal bottlenecking during the engraftment process by determining which specific sgRNAs were present in each tumor and allowing sgRNAs that did not successfully engraft to be excluded from analysis. A comparison of the sgRNA representation between $CD4^T$ positive and $CD4^T$ induced cells could then be performed to identify robustly depleted sgRNAs in the $CD4^T$ induced population. While performing *in vivo* pooled CRISPR screens poses several challenges, utilizing a focused sgRNA library with UMI barcodes and sorting $CD4^T$ induced cells prior to sequencing analysis would overcome many of these concerns.

Together, these methods constitute a core enabling technology for *in vivo* functional genomics in PDXs, allowing interrogation of gene essentiality, candidate drug targets, mechanisms of acquired resistance, tumor suppressor function, chemical:genetic interactions, and variants of unknown significance in

this tumor model. Ultimately, we hope that the novel preclinical modeling platform developed and validated in this thesis project can be applied broadly to define new therapeutic approaches for better cancer care.

BIBLIOGRAPHY

Ablain, J., Durand, E.M., Yang, S., Zhou, Y., and Zon, L.I. (2015). A CRISPR/Cas9 vector system for tissue-specific gene disruption in zebrafish. Dev. Cell *32*, 756–764.

Abudayyeh, O.O., Gootenberg, J.S., Konermann, S., Joung, J., Slaymaker, I.M., Cox, D.B.T., Shmakov, S., Makarova, K.S., Semenova, E., Minakhin, L., et al. (2016). C2c2 is a single-component programmable RNA-guided RNA-targeting CRISPR effector. Science *353*, aaf5573.

Agliano, A., Martin-Padura, I., Mancuso, P., Marighetti, P., Rabascio, C., Pruneri, G., Shultz, L.D., and Bertolini, F. (2008). Human acute leukemia cells injected in NOD/LtSz-scid/IL-2Rgamma null mice generate a faster and more efficient disease compared to other NOD/scid-related strains. Int. J. Cancer *123*, 2222–2227.

Aguirre, A.J., Meyers, R.M., Weir, B.A., Vazquez, F., Zhang, C.-Z., Ben-David, U., Cook, A., Ha, G., Harrington, W.F., Doshi, M.B., et al. (2016). Genomic copy number dictates a gene-independent cell response to CRISPR-Cas9 targeting. Cancer Discovery CD–16–0154.

Aparicio, S., Hidalgo, M., and Kung, A.L. (2015). Examining the utility of patient-derived xenograft mouse models. Nat. Rev. Cancer *15*, 311–316.

Aubrey, B.J., Kelly, G.L., Kueh, A.J., Brennan, M.S., O'Connor, L., Milla, L., Wilcox, S., Tai, L., Strasser, A., and Herold, M.J. (2015). An inducible lentiviral guide RNA platform enables the identification of tumor-essential genes and tumor-promoting mutations in vivo. Cell Rep *10*, 1422–1432.

Barrangou, R. (2012). RNA-mediated programmable DNA cleavage. Nat Biotechnol *30*, 836–838.

Barrangou, R., Fremaux, C., Deveau, H., Richards, M., Boyaval, P., Moineau, S., Romero, D.A., and Horvath, P. (2007). CRISPR provides acquired resistance against viruses in prokaryotes. Science *315*, 1709–1712.

Beard, C., Hochedlinger, K., Plath, K., Wutz, A., and Jaenisch, R. (2006). Efficient method to generate single-copy transgenic mice by site-specific integration in embryonic stem cells. Genesis *44*, 23–28.

Behan, F.M., Iorio, F., Picco, G., Gonçalves, E., Beaver, C.M., Migliardi, G., Santos, R., Rao, Y., Sassi, F., Pinnelli, M., et al. (2019). Prioritization of cancer therapeutic targets using CRISPR-Cas9 screens. Nature *568*, 511–516.

Ben-David, U., Beroukhim, R., and Golub, T.R. (2019). Genomic evolution of cancer models: perils and opportunities. Nat. Rev. Cancer 1–13.

Ben-David, U., Ha, G., Tseng, Y.-Y., Greenwald, N.F., Oh, C., Shih, J., McFarland, J.M., Wong, B., Boehm, J.S., Beroukhim, R., et al. (2017). Patient-derived xenografts undergo mouse-specific tumor evolution. Nature Publishing Group *49*, 1567–1575.

Bertotti, A., Migliardi, G., Galimi, F., Sassi, F., Torti, D., Isella, C., Cora, D., Di Nicolantonio, F., Buscarino, M., Petti, C., et al. (2011). A Molecularly Annotated Platform of Patient-Derived Xenografts ("Xenopatients") Identifies HER2 as an Effective Therapeutic Target in Cetuximab-Resistant Colorectal Cancer. Cancer Discovery *1*, 508–523.

Beshiri, M.L., Tice, C.M., Tran, C., Nguyen, H.M., Sowalsky, A.G., Agarwal, S., Jansson, K.H., Yang, Q., McGowen, K.M., Yin, J., et al. (2018). A PDX/Organoid Biobank of Advanced Prostate Cancers Captures Genomic and Phenotypic Heterogeneity for Disease Modeling and Therapeutic Screening. Clin. Cancer Res. *24*, 4332–4345.

Blasco, R.B., Karaca, E., Ambrogio, C., Cheong, T.-C., Karayol, E., Minero, V.G., Voena, C., and Chiarle, R. (2014). Simple and rapid in vivo generation of chromosomal rearrangements using CRISPR/Cas9 technology. Cell Rep *9*, 1219–1227.

Bolotin, A., Quinquis, B., Sorokin, A., and Ehrlich, S.D. (2005). Clustered regularly interspaced short palindrome repeats (CRISPRs) have spacers of extrachromosomal origin. Microbiology (Reading, Engl.) *151*, 2551–2561.

Bonini, C., Ferrari, G., Verzeletti, S., Servida, P., Zappone, E., Ruggieri, L., Ponzoni, M., Rossini, S., Mavilio, F., Traversari, C., et al. (1997). HSV-TK gene transfer into donor lymphocytes for control of allogeneic graft-versus-leukemia. Science *276*, 1719–1724.

Bossi, D., Cicalese, A., Dellino, G.I., Luzi, L., Riva, L., D'Alesio, C., Diaferia, G.R., Carugo, A., Cavallaro, E., Piccioni, R., et al. (2016). In vivo genetic screens of patient-derived tumors revealed unexpected frailty of the transformed phenotype. Cancer Discovery CD–15–1200.

Brinkman, E.K., Chen, T., Amendola, M., and van Steensel, B. (2014). Easy quantitative assessment of genome editing by sequence trace decomposition. Nucleic Acids Research *42*, e168–e168.

Brun, S., Faucon-Biguet, N., and Mallet, J. (2003). Optimization of transgene expression at the posttranscriptional level in neural cells: implications for gene therapy. Mol. Ther. *7*, 782–789.

Bruna, A., Rueda, O.M., Greenwood, W., Batra, A.S., Callari, M., Batra, R.N., Pogrebniak, K., Sandoval, J., Cassidy, J.W., Tufegdzic-Vidakovic, A., et al. (2016). A Biobank of Breast Cancer Explants with Preserved Intra-tumor Heterogeneity to Screen Anticancer Compounds. Cell.

Calles, A., Rubio-Viqueira, B., and Hidalgo, M. (2013). Primary human non-small cell lung and pancreatic tumorgraft models--utility and applications in drug discovery and tumor biology. Curr Protoc Pharmacol *Chapter 14*, Unit14.26–14.26.21.

Campeau, E., Ruhl, V.E., Rodier, F., Smith, C.L., Rahmberg, B.L., Fuss, J.O., Campisi, J., Yaswen, P., Cooper, P.K., and Kaufman, P.D. (2009). A Versatile Viral System for Expression and Depletion of Proteins in Mammalian Cells. PLoS ONE *4*, e6529–18.

Cancer Genome Atlas Research Network, Weinstein, J.N., Collisson, E.A., Mills, G.B., Shaw, K.R.M., Ozenberger, B.A., Ellrott, K., Shmulevich, I., Sander, C., and Stuart, J.M. (2013). The Cancer Genome Atlas Pan-Cancer analysis project. Nature Publishing Group *45*, 1113–1120.

Cao, J., Wu, L., Zhang, S.-M., Lu, M., Cheung, W.K.C., Cai, W., Gale, M., Xu, Q., and Yan, Q. (2016). An easy and efficient inducible CRISPR/Cas9 platform with improved specificity for multiple gene targeting. Nucleic Acids Research *60*, gkw660–10.

Carroll, D. (2012). A CRISPR approach to gene targeting. Mol. Ther. *20*, 1658–1660.

Casini, A., Olivieri, M., Petris, G., Montagna, C., Reginato, G., Maule, G., Lorenzin, F., Prandi, D., Romanel, A., Demichelis, F., et al. (2018). A highly specific SpCas9 variant is identified by in vivo screening in yeast. Nature Publishing Group *36*, 265–271.

Cawthorne, C., Swindell, R., Stratford, I.J., Dive, C., and Welman, A. (2007). Comparison of doxycycline delivery methods for Tet-inducible gene expression in a subcutaneous xenograft model. J Biomol Tech *18*, 120–123.

Chang, M.T., Bhattarai, T.S., Schram, A.M., Bielski, C.M., Donoghue, M.T.A., Jonsson, P., Chakravarty, D., Phillips, S., Kandoth, C., Penson, A., et al. (2018). Accelerating Discovery of Functional Mutant Alleles in Cancer. Cancer Discovery *8*, 174–183.

Charles, J.P., Fuchs, J., Hefter, M., Vischedyk, J.B., Kleint, M., Vogiatzi, F., Schäfer, J.A., Nist, A., Timofeev, O., Wanzel, M., et al. (2014). Monitoring the dynamics of clonal tumour evolution in vivo using secreted luciferases. Nat Commun *5*, 3981.

Charlesworth, C.T., Deshpande, P.S., Dever, D.P., Camarena, J., Lemgart, V.T., Cromer, M.K., Vakulskas, C.A., Collingwood, M.A., Zhang, L., Bode, N.M., et al. (2019). Identification of preexisting adaptive immunity to Cas9 proteins in humans. Nat. Med. *25*, 249–254.

Chen, B., Gilbert, L.A., Cimini, B.A., Schnitzbauer, J., Zhang, W., Li, G.-W., Park,

J., Blackburn, E.H., Weissman, J.S., Qi, L.S., et al. (2013). Dynamic imaging of genomic loci in living human cells by an optimized CRISPR/Cas system. Cell *155*, 1479–1491.

Cheng, D.T., Mitchell, T.N., Zehir, A., Shah, R.H., Benayed, R., Syed, A., Chandramohan, R., Liu, Z.Y., Won, H.H., Scott, S.N., et al. (2015). Memorial Sloan Kettering-Integrated Mutation Profiling of Actionable Cancer Targets (MSK-IMPACT): A Hybridization Capture-Based Next-Generation Sequencing Clinical Assay for Solid Tumor Molecular Oncology. J Mol Diagn *17*, 251–264.

Choi, Y., Lee, S., Kim, K., Kim, S.-H., Chung, Y.-J., and Lee, C. (2018). Studying cancer immunotherapy using patient-derived xenografts (PDXs) in humanized mice. Exp. Mol. Med. *50*, 99.

Chong, C.R., and Jänne, P.A. (2013). The quest to overcome resistance to EGFR-targeted therapies in cancer. Nat. Med. *19*, 1389–1400.

Cobb, L.M. (1973). The behaviour of carcinoma of the large bowel in man following transplantation into immune deprived mice. Br. J. Cancer *28*, 400–411.

Cong, L., Ran, F.A., Cox, D., Lin, S., Barretto, R., Habib, N., Hsu, P.D., Wu, X., Jiang, W., Marraffini, L.A., et al. (2013). Multiplex genome engineering using CRISPR/Cas systems. Science *339*, 819–823.

Cook, P.J., Thomas, R., Kannan, R., de Leon, E.S., Drilon, A., Rosenblum, M.K., Scaltriti, M., Benezra, R., and Ventura, A. (2017). Somatic chromosomal engineering identifies BCAN-NTRK1 as a potent glioma driver and therapeutic target. Nat Commun *8*, 15987.

Cottu, P., Bieche, I., Assayag, F., Botty, El, R., Chateau-Joubert, S., Thuleau, A., Bagarre, T., Albaud, B., Rapinat, A., Gentien, D., et al. (2014). Acquired Resistance to Endocrine Treatments Is Associated with Tumor-Specific Molecular Changes in Patient-Derived Luminal Breast Cancer Xenografts. Clin. Cancer Res. *20*, 4314–4325.

Dammert, M.A., Brägelmann, J., Olsen, R.R., Böhm, S., Monhasery, N., Whitney, C.P., Chalishazar, M.D., Tumbrink, H.L., Guthrie, M.R., Klein, S., et al. (2019). MYC paralog-dependent apoptotic priming orchestrates a spectrum of vulnerabilities in small cell lung cancer. Nat Commun *10*, 3485–11.

Daniel, V.C., Marchionni, L., Hierman, J.S., Rhodes, J.T., Devereux, W.L., Rudin, C.M., Yung, R., Parmigiani, G., Dorsch, M., Peacock, C.D., et al. (2009). A primary xenograft model of small-cell lung cancer reveals irreversible changes in gene expression imposed by culture in vitro. Cancer Res. *69*, 3364–3373.

Das, A.T., Tenenbaum, L., and Berkhout, B. (2016). Tet-On Systems For Doxycycline-inducible Gene Expression. Curr Gene Ther *16*, 156–167.

Datlinger, P., Rendeiro, A.F., Schmidl, C., Krausgruber, T., Traxler, P., Klughammer, J., Schuster, L.C., Kuchler, A., Alpar, D., and Bock, C. (2017). Pooled CRISPR screening with single-cell transcriptome readout. Nat. Methods *14*, 297–301.

Davis, K.M., Pattanayak, V., Thompson, D.B., Zuris, J.A., and Liu, D.R. (2015). Small molecule-triggered Cas9 protein with improved genome-editing specificity. Nature Chemical Biology *11*, 316–318.

Deltcheva, E., Chylinski, K., Sharma, C.M., Gonzales, K., Chao, Y., Pirzada, Z.A., Eckert, M.R., Vogel, J., and Charpentier, E. (2011). CRISPR RNA maturation by trans-encoded small RNA and host factor RNase III. Nature *471*, 602–607.

DeRose, Y.S., Wang, G., Lin, Y.-C., Bernard, P.S., Buys, S.S., Ebbert, M.T.W., Factor, R., Matsen, C., Milash, B.A., Nelson, E., et al. (2011). Tumor grafts derived from women with breast cancer authentically reflect tumor pathology, growth, metastasis and disease outcomes. Nat. Med. *17*, 1514–1520.

Deveau, H., Barrangou, R., Garneau, J.E., Labonté, J., Fremaux, C., Boyaval, P., Romero, D.A., Horvath, P., and Moineau, S. (2008). Phage response to CRISPR-encoded resistance in Streptococcus thermophilus. J. Bacteriol. *190*, 1390–1400.

Dickins, R.A., Hemann, M.T., Zilfou, J.T., Simpson, D.R., Ibarra, I., Hannon, G.J., and Lowe, S.W. (2005). Probing tumor phenotypes using stable and regulated synthetic microRNA precursors. Nat. Genet. *37*, 1289–1295.

Dijkstra, K.K., Cattaneo, C.M., Weeber, F., Chalabi, M., van de Haar, J., Fanchi, L.F., Slagter, M., van der Velden, D.L., Kaing, S., Kelderman, S., et al. (2018). Generation of Tumor-Reactive T Cells by Co-culture of Peripheral Blood Lymphocytes and Tumor Organoids. Cell *174*, 1586–1598.e12.

Dixit, A., Parnas, O., Li, B., Chen, J., Fulco, C.P., Jerby-Arnon, L., Marjanovic, N.D., Dionne, D., Burks, T., Raychowdhury, R., et al. (2016). Perturb-Seq: Dissecting Molecular Circuits with Scalable Single-Cell RNA Profiling of Pooled Genetic Screens. Cell *167*, 1853–1866.e17.

Doench, J.G. (2018). Am I ready for CRISPR? A user's guide to genetic screens. Nat. Rev. Genet. *19*, 67–80.

Doench, J.G., Fusi, N., Sullender, M., Hegde, M., Vaimberg, E.W., Donovan, K.F., Smith, I., Tothova, Z., Wilen, C., Orchard, R., et al. (2016). Optimized sgRNA design to maximize activity and minimize off-target effects of CRISPR-Cas9. Nat Biotechnol.

Dominguez, A.A., Lim, W.A., and Qi, L.S. (2016). Beyond editing: repurposing CRISPR-Cas9 for precision genome regulation and interrogation. Nat. Rev. Mol. Cell Biol. *17*, 5–15.

Dow, L.E., Fisher, J., O'Rourke, K.P., Muley, A., Kastenhuber, E.R., Livshits, G., Tschaharganeh, D.F., Socci, N.D., and Lowe, S.W. (2015). Inducible in vivo genome editing with CRISPR-Cas9. Nat Biotechnol *33*, 390–394.

Dow, L.E., Nasr, Z., Saborowski, M., Ebbesen, S.H., Manchado, E., Tasdemir, N., Lee, T., Pelletier, J., and Lowe, S.W. (2014). Conditional Reverse Tet-Transactivator Mouse Strains for the Efficient Induction of TRE-Regulated Transgenes in Mice. PLoS ONE *9*, e95236–11.

Dow, L.E., Premsrirut, P.K., Zuber, J., Fellmann, C., McJunkin, K., Miething, C., Park, Y., Dickins, R.A., Hannon, G.J., and Lowe, S.W. (2012). A pipeline for the generation of shRNA transgenic mice. Nat Protoc *7*, 374–393.

Drapkin, B.J., George, J., Christensen, C.L., Mino-Kenudson, M., Dries, R., Sundaresan, T., Phat, S., Myers, D.T., Zhong, J., Igo, P., et al. (2018). Genomic and Functional Fidelity of Small Cell Lung Cancer Patient-Derived Xenografts. Cancer Discovery *8*, 600–615.

Eirew, P., Steif, A., Khattra, J., Ha, G., Yap, D., Farahani, H., Gelmon, K., Chia, S., Mar, C., Wan, A., et al. (2015). Dynamics of genomic clones in breast cancer patient xenografts at single-cell resolution. Nature *518*, 422–426.

Eswaraka, J., and Giddabasappa, A. (2016). Chapter 6 - Humanized Mice and PDX Models (Elsevier Inc.).

Fichtner, I., Rolff, J., Soong, R., Hoffmann, J., Hammer, S., Sommer, A., Becker, M., and Merk, J. (2008). Establishment of patient-derived non-small cell lung cancer xenografts as models for the identification of predictive biomarkers. Clin. Cancer Res. *14*, 6456–6468.

Findlay, G.M., Boyle, E.A., Hause, R.J., Klein, J.C., and Shendure, J. (2014). Saturation editing of genomic regions by multiplex homology-directed repair. Nature *513*, 120–123.

Flanagan, S.P. (1966). “Nude,” a new hairless gene with pleiotropic effects in the mouse. Genet. Res. *8*, 295–309.

Fogh, J., Fogh, J.M., and Orfeo, T. (1977). One hundred and twenty-seven cultured human tumor cell lines producing tumors in nude mice. JNCI Journal of the National Cancer Institute *59*, 221–226.

Gaines, P., and Wojchowski, D.M. (1999). pIRES-CD4t, a dicistronic expression vector for MACS- or FACS-based selection of transfected cells. Biotech. *26*, 683–688.

Gandara, D.R., Mack, P.C., Bult, C., Li, T., Lara, P.N., Riess, J.W., Astrow, S.H., Gandour-Edwards, R., Cooke, D.T., Yoneda, K.Y., et al. (2015). Bridging tumor genomics to patient outcomes through an integrated patient-derived xenograft

platform. Clin Lung Cancer *16*, 165–172.

Gangopadhyay, S.A., Cox, K.J., Manna, D., Lim, D., Maji, B., Zhou, Q., and Choudhary, A. (2019). Precision Control of CRISPR-Cas9 Using Small Molecules and Light. Biochemistry *58*, 234–244.

Gao, H., Korn, J.M., Ferretti, S., Monahan, J.E., Wang, Y., Singh, M., Zhang, C., Schnell, C., Yang, G., Zhang, Y., et al. (2015). High-throughput screening using patient-derived tumor xenografts to predict clinical trial drug response. Nat. Med.

Gardner, E.E., Lok, B.H., Schneeberger, V.E., Desmeules, P., Miles, L.A., Arnold, P.K., Ni, A., Khodos, I., de Stanchina, E., Nguyen, T., et al. (2017). Chemosensitive Relapse in Small Cell Lung Cancer Proceeds through an EZH2-SLFN11 Axis. Cancer Cell *31*, 286–299.

Garneau, J.E., Dupuis, M.-È., Villion, M., Romero, D.A., Barrangou, R., Boyaval, P., Fremaux, C., Horvath, P., Magadán, A.H., and Moineau, S. (2010). The CRISPR/Cas bacterial immune system cleaves bacteriophage and plasmid DNA. Nature *468*, 67–71.

Gasiunas, G., Barrangou, R., Horvath, P., and Siksnys, V. (2012). Cas9-crRNA ribonucleoprotein complex mediates specific DNA cleavage for adaptive immunity in bacteria. Proc. Natl. Acad. Sci. U.S.a. *109*, E2579–E2586.

Gazdar, A.F., Bunn, P.A., and Minna, J.D. (2017). Small-cell lung cancer: what we know, what we need to know and the path forward. Nat. Rev. Cancer *893*, 1.

Gilbert, L.A., Horlbeck, M.A., Adamson, B., Villalta, J.E., Chen, Y., Whitehead, E.H., Guimaraes, C., Panning, B., Ploegh, H.L., Bassik, M.C., et al. (2014). Genome-Scale CRISPR-Mediated Control of Gene Repression and Activation. Cell *159*, 647–661.

Giovanella, B.C., Yim, S.O., Stehlin, J.S., and Williams, L.J. (1972). Development of invasive tumors in the “nude” mouse after injection of cultured human melanoma cells. JNCI Journal of the National Cancer Institute *48*, 1531–1533.

González, F., Zhu, Z., Shi, Z.-D., Lelli, K., Verma, N., Li, Q.V., and Huangfu, D. (2014). An iCRISPR Platform for Rapid, Multiplexable, and Inducible Genome Editing in Human Pluripotent Stem Cells. Stem Cell *15*, 215–226.

Gossen, M., Freundlieb, S., Bender, G., Müller, G., Hillen, W., and Bujard, H. (1995). Transcriptional activation by tetracyclines in mammalian cells. Science *268*, 1766–1769.

Gray, J.T., and Zolotukhin, S. (2011). Design and construction of functional AAV vectors. Methods Mol. Biol. *807*, 25–46.

Guerrera, F., Tabbò, F., Bessone, L., Maletta, F., Gaudiano, M., Ercole, E.,

Annaratone, L., Todaro, M., Boita, M., Filosso, P.L., et al. (2016). The Influence of Tissue Ischemia Time on RNA Integrity and Patient-Derived Xenografts (PDX) Engraftment Rate in a Non-Small Cell Lung Cancer (NSCLC) Biobank. PLoS ONE *11*, e0145100.

Guo, S., Qian, W., Cai, J., Zhang, L., Wery, J.-P., and Li, Q.-X. (2016). Molecular Pathology of Patient Tumors, Patient-Derived Xenografts, and Cancer Cell Lines. Cancer Res. *76*, 4619–4626.

Han, K., Jeng, E.E., Hess, G.T., Morgens, D.W., Li, A., and Bassik, M.C. (2017). Synergistic drug combinations for cancer identified in a CRISPR screen for pairwise genetic interactions. Nature Publishing Group *35*, 463–474.

Hanahan, D., Weinberg, R.A., and Hanahan, D. (2011). Hallmarks of Cancer: The Next Generation. Cell *144*, 646–674.

Heinz, N., Schambach, A., Galla, M., Maetzig, T., Baum, C., Loew, R., and Schiedlmeier, B. (2011). Retroviral and Transposon-Based Tet-Regulated All-In-One Vectors with Reduced Background Expression and Improved Dynamic Range. Human Gene Therapy *22*, 166–176.

Helling, B., König, M., Dälken, B., Engling, A., Krömer, W., Heim, K., Wallmeier, H., Haas, J., Wildemann, B., Fritz, B., et al. (2015). A specific CD4 epitope bound by tregalizumab mediates activation of regulatory T cells by a unique signaling pathway. Immunol. Cell Biol. *93*, 396–405.

Herbst, R.S., Morgensztern, D., and Boshoff, C. (2018). The biology and management of non-small cell lung cancer. Nature *553*, 446–454.

Hidalgo, M., Amant, F., Biankin, A.V., Budinska, E., Byrne, A.T., Caldas, C., Clarke, R.B., de Jong, S., Jonkers, J., Maelandsmo, G.M., et al. (2014). Patient-Derived Xenograft Models: An Emerging Platform for Translational Cancer Research. Cancer Discovery *4*, 998–1013.

Hilton, I.B., D'Ippolito, A.M., Vockley, C.M., Thakore, P.I., Crawford, G.E., Reddy, T.E., and Gersbach, C.A. (2015). Epigenome editing by a CRISPR-Cas9-based acetyltransferase activates genes from promoters and enhancers. Nat Biotechnol *33*, 510–517.

Hirenallur-Shanthappa, D.K., Ramírez, J.A., and Iritani, B.M. (2016). Chapter 5 - Immunodeficient Mice: The Backbone of Patient-Derived Tumor Xenograft Models (Elsevier Inc.).

Hodgkinson, C.L., Morrow, C.J., Li, Y., Metcalf, R.L., Rothwell, D.G., Trapani, F., Polanski, R., Burt, D.J., Simpson, K.L., Morris, K., et al. (2014). Tumorigenicity and genetic profiling of circulating tumor cells in small-cell lung cancer. Nat. Med. *20*, 897–903.

Hoffman, R.M. (2015). Patient-derived orthotopic xenografts: better mimic of metastasis than subcutaneous xenografts. Nat. Rev. Cancer *15*, 451–452.

Horlbeck, M.A., Xu, A., Wang, M., Bennett, N.K., Park, C.Y., Bogdanoff, D., Adamson, B., Chow, E.D., Kampmann, M., Peterson, T.R., et al. (2018). Mapping the Genetic Landscape of Human Cells. Cell *174*, 953–967.e22.

Horvath, P., and Barrangou, R. (2010). CRISPR/Cas, the immune system of bacteria and archaea. Science *327*, 167–170.

Hsu, P.D., Lander, E.S., and Zhang, F. (2014). Development and applications of CRISPR-Cas9 for genome engineering. Cell *157*, 1262–1278.

Hu, J.H., Miller, S.M., Geurts, M.H., Tang, W., Chen, L., Sun, N., Zeina, C.M., Gao, X., Rees, H.A., Lin, Z., et al. (2018). Evolved Cas9 variants with broad PAM compatibility and high DNA specificity. Nature *556*, 57–63.

Ipsaro, J.J., Shen, C., Arai, E., Xu, Y., Kinney, J.B., Joshua-Tor, L., Vakoc, C.R., and Shi, J. (2017). Rapid generation of drug-resistance alleles at endogenous loci using CRISPR-Cas9 indel mutagenesis. PLoS ONE *12*, e0172177–16.

Ishikawa, F., Yasukawa, M., Lyons, B., Yoshida, S., Miyamoto, T., Yoshimoto, G., Watanabe, T., Akashi, K., Shultz, L.D., and Harada, M. (2005). Development of functional human blood and immune systems in NOD/SCID/IL2 receptor {gamma} chain(null) mice. Blood *106*, 1565–1573.

Izumchenko, E., Paz, K., Ciznadija, D., Sloma, I., Katz, A., Vasquez-Dunddel, D., Ben-Zvi, I., Stebbing, J., McGuire, W., Harris, W., et al. (2017). Patient-derived xenografts effectively capture responses to oncology therapy in a heterogeneous cohort of patients with solid tumors. Ann. Oncol. *28*, 2595–2605.

Jackson, S.A., McKenzie, R.E., Fagerlund, R.D., Kieper, S.N., Fineran, P.C., and Brouns, S.J.J. (2017). CRISPR-Cas: Adapting to change. Science *356*, eaal5056.

Jansen, R., Embden, J.D.A.V., Gaastra, W., and Schouls, L.M. (2002). Identification of genes that are associated with DNA repeats in prokaryotes. Mol. Microbiol. *43*, 1565–1575.

Jinek, M., Chylinski, K., Fonfara, I., Hauer, M., Doudna, J.A., and Charpentier, E. (2012). A programmable dual-RNA-guided DNA endonuclease in adaptive bacterial immunity. Science *337*, 816–821.

Jinek, M., East, A., Cheng, A., Lin, S., Ma, E., and Doudna, J. (2013). RNA-programmed genome editing in human cells. Elife *2*, e00471.

John, T., Kohler, D., Pintilie, M., Yanagawa, N., Pham, N.-A., Li, M., Panchal, D., Hui, F., Meng, F., Shepherd, F.A., et al. (2011). The ability to form primary tumor

xenografts is predictive of increased risk of disease recurrence in early-stage non-small cell lung cancer. Clin. Cancer Res. *17*, 134–141.

Johnson, J.I., Decker, S., Zaharevitz, D., Rubinstein, L.V., Venditti, J.M., Schepartz, S., Kalyandrug, S., Christian, M., Arbuck, S., Hollingshead, M., et al. (2001). Relationships between drug activity in NCI preclinical in vitro and in vivo models and early clinical trials. Br. J. Cancer *84*, 1424–1431.

Kabadi, A.M., Ousterout, D.G., Hilton, I.B., and Gersbach, C.A. (2014). Multiplex CRISPR/Cas9-based genome engineering from a single lentiviral vector. Nucleic Acids Research *42*, e147–e147.

Kearns, N.A., Pham, H., Tabak, B., Genga, R.M., Silverstein, N.J., Garber, M., and Maehr, R. (2015). Functional annotation of native enhancers with a Cas9-histone demethylase fusion. Nat. Methods *12*, 401–403.

Kiani, S., Beal, J., Ebrahimkhani, M.R., Huh, J., Hall, R.N., Xie, Z., Li, Y., and Weiss, R. (2014). CRISPR transcriptional repression devices and layered circuits in mammalian cells. Nat. Methods *11*, 723–726.

Kim, S., Bae, T., Hwang, J., and Kim, J.-S. (2017). Rescue of high-specificity Cas9 variants using sgRNAs with matched 5' nucleotides. Genome Biol. *18*, 218.

Kleinstiver, B.P., Pattanayak, V., Prew, M.S., Tsai, S.Q., Nguyen, N.T., Zheng, Z., and Joung, J.K. (2016). High-fidelity CRISPR-Cas9 nucleases with no detectable genome-wide off-target effects. Nature *529*, 490–495.

Komor, A.C., Badran, A.H., and Liu, D.R. (2017). CRISPR-Based Technologies for the Manipulation of Eukaryotic Genomes. Cell *168*, 20–36.

Komor, A.C., Kim, Y.B., Packer, M.S., Zuris, J.A., and Liu, D.R. (2016). Programmable editing of a target base in genomic DNA without double-stranded DNA cleavage. Nature *533*, 420–424.

Koretzky, G.A. (2010). Multiple roles of CD4 and CD8 in T cell activation. J. Immunol. *185*, 2643–2644.

Krepler, C., Sproesser, K., Brafford, P., Beqiri, M., Garman, B., Xiao, M., Shannan, B., Watters, A., Perego, M., Zhang, G., et al. (2017). A Comprehensive Patient-Derived Xenograft Collection Representing the Heterogeneity of Melanoma. Cell Rep *21*, 1953–1967.

Kumar, M., Keller, B., Makalou, N., and Sutton, R.E. (2001). Systematic Determination of the Packaging Limit of Lentiviral Vectors. Human Gene Therapy 1893–1905.

Kung, A.L. (2007). Practices and pitfalls of mouse cancer models in drug discovery. Adv. Cancer Res. *96*, 191–212.

Lallo, A., Schenk, M.W., Frese, K.K., Blackhall, F., and Dive, C. (2017). Circulating tumor cells and CDX models as a tool for preclinical drug development. Transl Lung Cancer Res *6*, 397–408.

Lander, E.S. (2016). The Heroes of CRISPR. Cell *164*, 18–28.

Lee, S.H., Hu, W., Matulay, J.T., Silva, M.V., Owczarek, T.B., Kim, K., Chua, C.W., Barlow, L.J., Kandoth, C., Williams, A.B., et al. (2018). Tumor Evolution and Drug Response in Patient-Derived Organoid Models of Bladder Cancer. Cell *173*, 515–528.e517.

Liao, H.-K., Hatanaka, F., Araoka, T., Reddy, P., Wu, M.-Z., Sui, Y., Yamauchi, T., Sakurai, M., O'Keefe, D.D., Núñez-Delicado, E., et al. (2017). In Vivo Target Gene Activation via CRISPR/Cas9-Mediated Trans-epigenetic Modulation. Cell *171*, 1495–1498.e14.

Lieber, M.R. (2010). The mechanism of double-strand DNA break repair by the nonhomologous DNA end-joining pathway. Annu. Rev. Biochem. *79*, 181–211.

Liu, K.I., Ramli, M.N.B., Woo, C.W.A., Wang, Y., Zhao, T., Zhang, X., Yim, G.R.D., Chong, B.Y., Gowher, A., Chua, M.Z.H., et al. (2016a). A chemical-inducible CRISPR–Cas9 system for rapid control of genome editing. Nature Chemical Biology *12*, 980–987.

Liu, X.S., Wu, H., Ji, X., Stelzer, Y., Wu, X., Czauderna, S., Shu, J., Dadon, D., Young, R.A., and Jaenisch, R. (2016b). Editing DNA Methylation in the Mammalian Genome. Cell *167*, 233–247.e17.

Loew, R., Heinz, N., Hampf, M., Bujard, H., and Gossen, M. (2010). Improved Tet-responsive promoters with minimized background expression. BMC Biotechnol *10*, 81.

Logan, A.C., Nightingale, S.J., Haas, D.L., Cho, G.J., Pepper, K.A., and Kohn, D.B. (2004). Factors influencing the titer and infectivity of lentiviral vectors. Human Gene Therapy *15*, 976–988.

Maddalo, D., Manchado, E., Concepcion, C.P., Bonetti, C., Vidigal, J.A., Han, Y.-C., Ogrodowski, P., Crippa, A., Rekhtman, N., de Stanchina, E., et al. (2014). In vivo engineering of oncogenic chromosomal rearrangements with the CRISPR/Cas9 system. Nature *516*, 423–427.

Maji, B., Moore, C.L., Zetsche, B., Volz, S.E., Zhang, F., Shoulders, M.D., and Choudhary, A. (2017). Multidimensional chemical control of CRISPR-Cas9. Nature Chemical Biology *13*, 9–11.

Makarova, K.S., Wolf, Y.I., Alkhnbashi, O.S., Costa, F., Shah, S.A., Saunders, S.J., Barrangou, R., Brouns, S.J.J., Charpentier, E., Haft, D.H., et al. (2015). An updated evolutionary classification of CRISPR-Cas systems. Nat. Rev. Microbiol.

13, 722–736.

Malaney, P., Nicosia, S.V., and Davé, V. (2014). One mouse, one patient paradigm: New avatars of personalized cancer therapy. Cancer Letters *344*, 1–12.

Mali, P., Aach, J., Stranges, P.B., Esvelt, K.M., Moosburner, M., Kosuri, S., Yang, L., and Church, G.M. (2013a). CAS9 transcriptional activators for target specificity screening and paired nickases for cooperative genome engineering. Nat Biotechnol *31*, 833–838.

Mali, P., Yang, L., Esvelt, K.M., Aach, J., Guell, M., DiCarlo, J.E., Norville, J.E., and Church, G.M. (2013b). RNA-guided human genome engineering via Cas9. Science *339*, 823–826.

Manchado, E., Weissmueller, S., Morris, J.P., Chen, C.-C., Wullenkord, R., Lujambio, A., de Stanchina, E., Poirier, J.T., Gainor, J.F., Corcoran, R.B., et al. (2016). A combinatorial strategy for treating KRAS-mutant lung cancer. Nature.

Mao, Z., Bozzella, M., Seluanov, A., and Gorbunova, V. (2008). Comparison of nonhomologous end joining and homologous recombination in human cells. DNA Repair (Amst.) *7*, 1765–1771.

Maresch, R., Mueller, S., Veltkamp, C., Öllinger, R., Friedrich, M., Heid, I., Steiger, K., Weber, J., Engleitner, T., Barenboim, M., et al. (2016). Multiplexed pancreatic genome engineering and cancer induction by transfection-based CRISPR/Cas9 delivery in mice. Nat Commun *7*, 10770.

Marraffini, L.A., and Sontheimer, E.J. (2008). CRISPR interference limits horizontal gene transfer in staphylococci by targeting DNA. Science *322*, 1843–1845.

Marraffini, L.A., and Sontheimer, E.J. (2010). CRISPR interference: RNA-directed adaptive immunity in bacteria and archaea. Nat. Rev. Genet. *11*, 181–190.

Mattar, M., Abdel-Wahab, O., Poirier, J.T., Scaltriti, M., and de Stanchina, E. (2016). Chapter 3 - Methodologies for Developing and Maintaining Patient-Derived Xenograft Mouse Models (Elsevier Inc.).

McDermott, S.P., Eppert, K., Lechman, E.R., Doedens, M., and Dick, J.E. (2010). Comparison of human cord blood engraftment between immunocompromised mouse strains. Blood *116*, 193–200.

McGranahan, N., and Swanton, C. (2017). Clonal Heterogeneity and Tumor Evolution: Past, Present, and the Future. Cell *168*, 613–628.

Meca-Cortés, O., Guerra-Rebollo, M., Garrido, C., Borrós, S., Rubio, N., and

Blanco, J. (2017). CRISPR/Cas9-Mediated Knockin Application in Cell Therapy: A Non-viral Procedure for Bystander Treatment of Glioma in Mice. Mol Ther Nucleic Acids *8*, 395–403.

Michlits, G., Hubmann, M., Wu, S.-H., Vainorius, G., Budusan, E., Zhuk, S., Burkard, T.R., Novatchkova, M., Aichinger, M., Lu, Y., et al. (2017). CRISPR-UMI: single-cell lineage tracing of pooled CRISPR-Cas9 screens. Nat. Methods *14*, 1191–1197.

Miles, L.A., Garippa, R.J., and Poirier, J.T. (2016). Design, execution, and analysis of pooled in vitro CRISPR/Cas9 screens. Febs J. *283*, 3170–3180.

Mojica, F.J., Díez-Villaseñor, C., Soria, E., and Juez, G. (2000). Biological significance of a family of regularly spaced repeats in the genomes of Archaea, Bacteria and mitochondria. Mol. Microbiol. *36*, 244–246.

Mojica, F.J.M., Díez-Villaseñor, C., García-Martínez, J., and Soria, E. (2005). Intervening sequences of regularly spaced prokaryotic repeats derive from foreign genetic elements. J. Mol. Evol. *60*, 174–182.

Monsma, D.J., Cherba, D.M., Eugster, E.E., Dylewski, D.L., Davidson, P.T., Peterson, C.A., Borgman, A.S., Winn, M.E., Dykema, K.J., Webb, C.P., et al. (2015). Melanoma patient derived xenografts acquire distinct Vemurafenib resistance mechanisms. Am J Cancer Res *5*, 1507–1518.

Morrow, C.J., Trapani, F., Metcalf, R.L., Bertolini, G., Hodgkinson, C.L., Khandelwal, G., Kelly, P., Galvin, M., Carter, L., Simpson, K.L., et al. (2016). Tumourigenic non-small-cell lung cancer mesenchymal circulating tumour cells: a clinical case study. Ann. Oncol. *27*, 1155–1160.

Neal, J.T., Li, X., Zhu, J., Giangarra, V., Grzeskowiak, C.L., Ju, J., Liu, I.H., Chiou, S.-H., Salahudeen, A.A., Smith, A.R., et al. (2018). Organoid Modeling of the Tumor Immune Microenvironment. Cell *175*, 1972–1988.e16.

Norman, T.M., Horlbeck, M.A., Replogle, J.M., Ge, A.Y., Xu, A., Jost, M., Gilbert, L.A., and Weissman, J.S. (2019). Exploring genetic interaction manifolds constructed from rich single-cell phenotypes. Science *365*, 786–793.

Oakes, B.L., Nadler, D.C., Flamholz, A., Fellmann, C., Staahl, B.T., Doudna, J.A., and Savage, D.F. (2016). Profiling of engineering hotspots identifies an allosteric CRISPR-Cas9 switch. Nat Biotechnol *34*, 646–651.

Oh, B.Y., Lee, W.Y., Jung, S., Hong, H.K., Nam, D.-H., Park, Y.A., Huh, J.W., Yun, S.H., Kim, H.C., Chun, H.-K., et al. (2015). Correlation between tumor engraftment in patient-derived xenograft models and clinical outcomes in colorectal cancer patients. Oncotarget *6*, 16059–16068.

Pantelouris, E.M. (1968). Absence of thymus in a mouse mutant. Nature *217*,

370–371.

Pillai, S.P.S., and Uthamanthil, R.K. (2016). Chapter 1 - PDX Models: History and Development (Elsevier Inc.).

Poirier, J.T., Gardner, E.E., Connis, N., Moreira, A.L., de Stanchina, E., Hann, C.L., and Rudin, C.M. (2015). DNA methylation in small cell lung cancer defines distinct disease subtypes and correlates with high expression of EZH2. Oncogene.

Poirier, J.T. (2017). CRISPR Libraries and Screening. Prog Mol Biol Transl Sci *152*, 69–82.

Polley, E., Kunkel, M., Evans, D., Silvers, T., Delosh, R., Laudeman, J., Ogle, C., Reinhart, R., Selby, M., Connelly, J., et al. (2016). Small Cell Lung Cancer Screen of Oncology Drugs, Investigational Agents, and Gene and microRNA Expression. J. Natl. Cancer Inst. *108*, djw122.

Pourcel, C., Salvignol, G., and Vergnaud, G. (2005). CRISPR elements in Yersinia pestis acquire new repeats by preferential uptake of bacteriophage DNA, and provide additional tools for evolutionary studies. Microbiology (Reading, Engl.) *151*, 653–663.

Puca, L., Bareja, R., Prandi, D., Shaw, R., Benelli, M., Karthaus, W.R., Hess, J., Sigouros, M., Donoghue, A., Kossai, M., et al. (2018). Patient derived organoids to model rare prostate cancer phenotypes. Nat Commun *9*, 2404.

Quintana, E., Shackleton, M., Sabel, M.S., Fullen, D.R., Johnson, T.M., and Morrison, S.J. (2008). Efficient tumour formation by single human melanoma cells. Nature *456*, 593–598.

Romero, R., Sayin, V.I., Davidson, S.M., Bauer, M.R., Singh, S.X., LeBoeuf, S.E., Karakousi, T.R., Ellis, D.C., Bhutkar, A., Sánchez-Rivera, F.J., et al. (2017). Keap1 loss promotes Kras-driven lung cancer and results in dependence on glutaminolysis. Nat. Med. *23*, 1362–1368.

Rose, J.C., Stephany, J.J., Valente, W.J., Trevillian, B.M., Dang, H.V., Bielas, J.H., Maly, D.J., and Fowler, D.M. (2017). Rapidly inducible Cas9 and DSB-ddPCR to probe editing kinetics. Nat. Methods *14*, 891–896.

Rosfjord, E., Lucas, J., Li, G., and Gerber, H.-P. (2014). Advances in patient-derived tumor xenografts: From target identification to predicting clinical response rates in oncology. Biochemical Pharmacology *91*, 135–143.

Rygaard, J., and Povlsen, C.O. (1969). Heterotransplantation of a human malignant tumour to “Nude” mice. Acta Pathol Microbiol Scand *77*, 758–760.

Sanjana, N.E., Shalem, O., and Zhang, F. (2014). Improved vectors and

genome-wide libraries for CRISPR screening. Nat. Methods *11*, 783–784.

Sastry, L., Johnson, T., Hobson, M.J., Smucker, B., and Cornetta, K. (2002). Titering lentiviral vectors: comparison of DNA, RNA and marker expression methods. Gene Ther *9*, 1155–1162.

Sánchez-Rivera, F.J., and Jacks, T. (2015). Applications of the CRISPR–Cas9 system in cancer biology. Nat. Rev. Cancer *15*, 387–395.

Sánchez-Rivera, F.J., Papagiannakopoulos, T., Romero, R., Tammela, T., Bauer, M.R., Bhutkar, A., Joshi, N.S., Subbaraj, L., Bronson, R.T., Xue, W., et al. (2014). Rapid modelling of cooperating genetic events in cancer through somatic genome editing. Nature *516*, 428–431.

Schneeberger, V.E., Allaj, V., Gardner, E.E., Poirier, J.T., and Rudin, C.M. (2016). Quantitation of Murine Stroma and Selective Purification of the Human Tumor Component of Patient-Derived Xenografts for Genomic Analysis. PLoS ONE *11*, e0160587.

Shalem, O., Sanjana, N.E., Hartenian, E., Shi, X., Scott, D.A., Mikkelsen, T.S., Heckl, D., Ebert, B.L., Root, D.E., Doench, J.G., et al. (2014). Genome-scale CRISPR-Cas9 knockout screening in human cells. Science *343*, 84–87.

Shi, J., Wang, E., Milazzo, J.P., Wang, Z., Kinney, J.B., and Vakoc, C.R. (2015). Discovery of cancer drug targets by CRISPR-Cas9 screening of protein domains. Nat Biotechnol *33*, 661–667.

Shmakov, S., Smargon, A., Scott, D., Cox, D., Pyzocha, N., Yan, W., Abudayyeh, O.O., Gootenberg, J.S., Makarova, K.S., Wolf, Y.I., et al. (2017). Diversity and evolution of class 2 CRISPR-Cas systems. Nat. Rev. Microbiol. *15*, 169–182.

Shorthouse, A.J., Smyth, J.F., Steel, G.G., Ellison, M., Mills, J., and Peckham, M.J. (1980). The human tumour xenograft--a valid model in experimental chemotherapy? Br J Surg *67*, 715–722.

Siegel, R.L., Miller, K.D., and Jemal, A. (2019). Cancer statistics, 2019. CA Cancer J Clin *69*, 7–34.

Siolas, D., and Hannon, G.J. (2013). Patient-Derived Tumor Xenografts: Transforming Clinical Samples into Mouse Models. Cancer Res. *73*, 5315–5319.

Sivanand, S., Peña-Llopis, S., Zhao, H., Kucejova, B., Spence, P., Pavia-Jimenez, A., Yamasaki, T., McBride, D.J., Gillen, J., Wolff, N.C., et al. (2012). A validated tumorgraft model reveals activity of dovitinib against renal cell carcinoma. Sci Transl Med *4*, 137ra75–137ra75.

Stoeckius, M., Hafemeister, C., Stephenson, W., Houck-Loomis, B., Chattopadhyay, P.K., Swerdlow, H., Satija, R., and Smibert, P. (2017).

Simultaneous epitope and transcriptome measurement in single cells. Nat. Methods *14*, 865–868.

Taki, T., and Taniwaki, M. (2006). Chromosomal translocations in cancer and their relevance for therapy. Curr Opin Oncol *18*, 62–68.

Tentler, J.J., Tan, A.C., Weekes, C.D., Jimeno, A., Leong, S., Pitts, T.M., Arcaroli, J.J., Messersmith, W.A., and Eckhardt, S.G. (2012). Patient-derived tumour xenografts as models for oncology drug development. Nat Rev Clin Oncol *9*, 338–350.

Thress, K.S., Paweletz, C.P., Felip, E., Cho, B.C., Stetson, D., Dougherty, B., Lai, Z., Markovets, A., Vivancos, A., Kuang, Y., et al. (2015). Acquired EGFR C797S mutation mediates resistance to AZD9291 in non-small cell lung cancer harboring EGFR T790M. Nat. Med. *21*, 560–562.

Townsend, E.C., Murakami, M.A., Christodoulou, A., Christie, A.L., Köster, J., DeSouza, T.A., Morgan, E.A., Kallgren, S.P., Liu, H., Wu, S.-C., et al. (2016). The Public Repository of Xenografts Enables Discovery and Randomized Phase II-like Trials in Mice. Cancer Cell *29*, 574–586.

Tschaharganeh, D.F., Lowe, S.W., Garippa, R.J., and Livshits, G. (2016). Using CRISPR/Cas to study gene function and model disease in vivo. Febs J. *283*, 3194–3203.

Tuveson, D., and Clevers, H. (2019). Cancer modeling meets human organoid technology. Science *364*, 952–955.

van Rijn, S., Nilsson, J., Noske, D.P., Vandertop, W.P., Tannous, B.A., and Würdinger, T. (2013). Functional multiplex reporter assay using tagged Gaussia luciferase. Sci Rep *3*, 1046.

Ventura, A., and Dow, L.E. (2018). Modeling Cancer in the CRISPR Era. Annu. Rev. Cancer Biol. *2*, 111–131.

Verma, N., Pan, H., Doré, L.C., Shukla, A., Li, Q.V., Pelham-Webb, B., Teijeiro, V., González, F., Krivtsov, A., Chang, C.-J., et al. (2017). TET proteins safeguard bivalent promoters from de novo methylation in human embryonic stem cells. Nat. Genet. *50*, 83–95.

Vlachogiannis, G., Hedayat, S., Vatsiou, A., Jamin, Y., Fernández-Mateos, J., Khan, K., Lampis, A., Eason, K., Huntingford, I., Burke, R., et al. (2018). Patient-derived organoids model treatment response of metastatic gastrointestinal cancers. Science *359*, 920–926.

Wang, M., Yao, L.-C., Cheng, M., Cai, D., Martinek, J., Pan, C.-X., Shi, W., Ma, A.-H., De Vere White, R.W., Airhart, S., et al. (2018). Humanized mice in studying efficacy and mechanisms of PD-1-targeted cancer immunotherapy.

Faseb J. *32*, 1537–1549.

Wang, R., Preamplume, G., Terns, M.P., Terns, R.M., and Li, H. (2011a). Interaction of the Cas6 riboendonuclease with CRISPR RNAs: recognition and cleavage. Structure *19*, 257–264.

Wang, T., Birsoy, K., Hughes, N.W., Krupczak, K.M., Post, Y., Wei, J.J., Lander, E.S., and Sabatini, D.M. (2015). Identification and characterization of essential genes in the human genome. Science *350*, 1096–1101.

Wang, T., Wei, J.J., Sabatini, D.M., and Lander, E.S. (2014). Genetic screens in human cells using the CRISPR-Cas9 system. Science *343*, 80–84.

Wang, X., Chang, W.-C., Wong, C.W., Colcher, D., Sherman, M., Ostberg, J.R., Forman, S.J., Riddell, S.R., and Jensen, M.C. (2011b). A transgene-encoded cell surface polypeptide for selection, in vivo tracking, and ablation of engineered cells. Blood *118*, 1255–1263.

Weeber, F., van de Wetering, M., Hoogstraat, M., Dijkstra, K.K., Krijgsman, O., Kuilman, T., Gadellaa-van Hooijdonk, C.G.M., van der Velden, D.L., Peeper, D.S., Cuppen, E.P.J.G., et al. (2015). Preserved genetic diversity in organoids cultured from biopsies of human colorectal cancer metastases. Proc. Natl. Acad. Sci. U.S.a. *112*, 13308–13311.

Wienert, B., Shin, J., Zelin, E., Pestal, K., and Corn, J.E. (2018). In vitro-transcribed guide RNAs trigger an innate immune response via the RIG-I pathway. PLoS Biol. *16*, e2005840.

Williams, S.A., Anderson, W.C., Santaguida, M.T., and Dylla, S.J. (2013). Patient-derived xenografts, the cancer stem cell paradigm, and cancer pathobiology in the 21st century. Lab. Invest. *93*, 970–982.

Winters, I.P., Chiou, S.-H., Paulk, N.K., McFarland, C.D., Lalgudi, P.V., Ma, R.K., Lisowski, L., Connolly, A.J., Petrov, D.A., Kay, M.A., et al. (2017). Multiplexed in vivo homology-directed repair and tumor barcoding enables parallel quantification of Kras variant oncogenicity. Nat Commun *8*, 2053.

Wroblewska, A., Dhainaut, M., Ben-Zvi, B., Rose, S.A., Park, E.S., Amir, E.-A.D., Bektesevic, A., Baccarini, A., Merad, M., Rahman, A.H., et al. (2018). Protein Barcodes Enable High-Dimensional Single-Cell CRISPR Screens. Cell *175*, 1141–1155.e16.

Wu, M., Liu, S., Gao, Y., Bai, H., Machairaki, V., Li, G., Chen, T., and Cheng, L. (2018). Conditional gene knockout and reconstitution in human iPSCs with an inducible Cas9 system. Stem Cell Research *29*, 6–14.

Xue, W., Chen, S., Yin, H., Tammela, T., Papagiannakopoulos, T., Joshi, N.S., Cai, W., Yang, G., Bronson, R., Crowley, D.G., et al. (2014). CRISPR-mediated

direct mutation of cancer genes in the mouse liver. Nature *514*, 380–384.

Zafra, M.P., Schatoff, E.M., Katti, A., Foronda, M., Breinig, M., Schweitzer, A.Y., Simon, A., Han, T., Goswami, S., Montgomery, E., et al. (2018). Optimized base editors enable efficient editing in cells, organoids and mice. Nat Biotechnol *36*, 888–893.

Zetsche, B., Volz, S.E., and Zhang, F. (2015). A split-Cas9 architecture for inducible genome editing and transcription modulation. Nature Publishing Group *33*, 139–142.

Zhang, B., Metharom, P., Jullie, H., Ellem, K.A., Cleghorn, G., West, M.J., and Wei, M.Q. (2004). The significance of controlled conditions in lentiviral vector titration and in the use of multiplicity of infection (MOI) for predicting gene transfer events. Genet Vaccines Ther *2*, 6.

Zhao, Y., Shuen, T.W.H., Toh, T.B., Chan, X.Y., Liu, M., Tan, S.Y., Fan, Y., Yang, H., Lyer, S.G., Bonney, G.K., et al. (2018). Development of a new patient-derived xenograft humanised mouse model to study human-specific tumour microenvironment and immunotherapy. Gut *67*, 1845–1854.

Zhou, X., Vink, M., Klaver, B., Berkhout, B., and Das, A.T. (2006). Optimization of the Tet-On system for regulated gene expression through viral evolution. Gene Ther *13*, 1382–1390.